Computer Physics Communications 302 (2024) 109243

Contents lists available at ScienceDirect

Computer Physics Communications

journal homepage: www.elsevier.com/locate/cpc

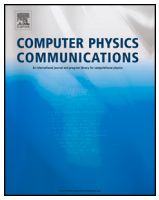

Computer Programs in Physics

Improvements in charged lepton and photon propagation for the software PROPOSAL ☆

Jean-Marco Alameddine [a,c,*], Johannes Albrecht [a,c], Hans Dembinski [a], Pascal Gutjahr [a,c], Karl-Heinz Kampert [b], Wolfgang Rhode [a,c], Maximilian Sackel [a], Alexander Sandrock [b], Jan Soedingrekso [a]

[a] TU Dortmund University, Department of Physics, Otto-Hahn-Straße 4a, 44227 Dortmund, Germany
[b] University of Wuppertal, School of Mathematics and Natural Sciences, Gaußstraße 20, 42119 Wuppertal, Germany
[c] Lamarr Institute for Machine Learning and Artificial Intelligence, Joseph-von-Fraunhofer-Straße 25, 44227 Dortmund, Germany

ARTICLE INFO

Dataset link: 10.17632/g478pjdcxy.2

Keywords:
Monte-Carlo simulation
Muon interaction
Tau propagation
Air shower
Electromagnetic interaction
Astroparticle physics

ABSTRACT

Accurate particle simulations are essential for the next generation of experiments in astroparticle physics. The Monte Carlo simulation library PROPOSAL is a flexible tool to efficiently propagate high-energy leptons and photons through large volumes of media, for example in the context of underground observatories. It is written as a C++ library, including a Python interface. In this paper, the most recent updates of PROPOSAL are described, including the addition of electron, positron, and photon propagation, for which new interaction types have been implemented. This allows the usage of PROPOSAL to simulate electromagnetic particle cascades, for example in the context of air shower simulations. The precision of the propagation has been improved by including rare interaction processes, new photonuclear parametrizations, deflections in stochastic interactions, and the possibility of propagating in inhomogeneous density distributions. Additional technical improvements regarding the interpolation routine and the propagation algorithm are described.

New version program summary

Program Title: PROPOSAL.
CPC Library link to program files: https://doi.org/10.17632/g478pjdcxy.2.
Developer's repository link: https://github.com/tudo-astroparticlephysics/PROPOSAL.
Licensing provisions: LGPL.
Programming language: C++, Python.
Journal reference of previous version: Comput. Phys. Commun. 242 (2019) 132.
Does the new version supersede the previous version?: Yes.
Reasons for the new version: Substantial addition of features. Various bugfixes.
Summary of revisions: The library now also treats photons and has the corresponding processes implemented. New parametrizations for photonuclear interaction have been implemented. The angular deflection in stochastic energy losses has been implemented in addition to the already existing multiple scattering implementation, which has been improved to reduce the runtime. The implementation of the Landau-Pomeranchuk-Migdal effect has been corrected. The propagation algorithm has been improved, including the support of inhomogeneous density distributions.
Nature of problem: Three-dimensional propagation of charged leptons and photons through different media. Particles lose energy stochastically by ionization, bremsstrahlung, pair production, and photonuclear interaction for charged leptons (including annihilation with atomic electrons for positrons) and Compton scattering, pair production, photoelectric effect and photohadronic interaction for photons. Additionally, they are deflected while propagating through the medium due to both multiple elastic Coulomb scattering as well as deflections in individual stochastic interactions. Unstable particles eventually decay, producing secondary particles.
Solution method: Monte-Carlo simulation. The library samples the next interaction point, the type of interaction process, the energy lost in this interaction process, and the energy lost until this point. Particles are propagated

☆ The review of this paper was arranged by Prof. Z. Was.

* Corresponding author.
E-mail address: jean-marco.alameddine@udo.edu (J.-M. Alameddine).

https://doi.org/10.1016/j.cpc.2024.109243
Received 21 November 2023; Received in revised form 6 May 2024; Accepted 10 May 2024
Available online 15 May 2024

until they decay, lose all their kinetic energy (for photons: reach a lower energy limit defined by the validity of the underlying cross sections), or until a user-defined termination criterion is reached. For each propagation step, the angular deflection and endpoint shift due to multiple scattering is calculated.
To improve the performance and deal with the divergence of the bremsstrahlung cross section for small photon energies, energy losses below a predefined relative or absolute energy threshold are treated continuously. The computation time is improved by the use of interpolation tables.

1. Introduction

PROPOSAL is a C++ and Python software library, simulating the stochastic propagation of high-energy charged leptons using Monte Carlo methods [1]. It was initially designed to propagate atmospheric or neutrino-induced muons as well as tau leptons through large volumes in the context of underground experiments, replacing the Java-written simulation software MMC [2]. Other existing muon simulation tools are MUSIC [3], MUM [4], and the backward simulation software PUMAS [5]. While each code has its advantages and specialties, the unique feature of PROPOSAL is its flexibility, allowing a detailed customization of the propagation environment, including a choice for the physics parametrizations themselves. Furthermore, PROPOSAL is capable of providing accurate, yet efficient particle simulations. This is achieved by the underlying propagation algorithm, which intrinsically allows for large propagation steps; the usage of optimized interpolation tables to accelerate the underlying calculations; and steering possibilities for the user to find a trade-off between performance and precision for each simulation. These features are especially relevant for applications where particles are propagated over large distances. As a consequence, PROPOSAL has been utilized in a wide range of use cases, including neutrino observatories such as IceCube [6] and KM3NeT [7,8], radio neutrino simulations [9], or dark matter underground experiments [10].

This article describes the improvements made in PROPOSAL since its last update [11], including photon propagation and the improvement of electron and positron propagation in the context of air shower simulations as the main feature. In Section 2, improvements of the muon propagation, including the implementation of muon deflections in stochastic interactions, are presented. In Section 3, the implementation of high-energy electron, positron, and photon interactions is described. Section 4 describes the new options for retrieving individual secondary particles from the existing propagation output. The inclusion of particle propagation in inhomogeneous density distributions is described in Section 5. Further technical improvements, including a new interpolation method, improvements in the propagation routine, and a description of the current installation process, are discussed in Section 6 before a conclusion is given in Section 7.

2. Improved muon interactions

The accuracy of the relevant muon interactions above GeV energies, i.e., ionization, bremsstrahlung, pair production, and photonuclear interaction, was already on a high level during the initial developments in MMC and has since then continuously been improved. The theoretical uncertainties of the combined energy loss cross sections are on a percent or sub-percent level, considering even Coulomb corrections and one-loop diagrams, see [12]. However, due to the large amount of atmospheric muons measured in detectors at the Earth's surface or underground, even rare interactions can occur in significant numbers. The consideration of rare scenarios and reduction of uncertainties not only for the energy loss but also for the deflection is getting more relevant as detection and reconstruction methods continuously improve. Therefore, PROPOSAL has improved its muon simulation, including rare interactions, new photonuclear parametrizations, and stochastic deflections, as described in this section. In addition, an issue in the parametrization of the Landau-Pomeranchuk-Migdal effect has been resolved. Fig. 1 shows an overview of all muon energy loss processes currently implemented in PROPOSAL.

2.1. Rare interactions: $\mu^+\mu^-$ pair production and weak interaction

The production of a $\mu^+\mu^-$ pair only contributes a fraction no more than $\approx 10^{-3}$ to the total energy loss of muons and is, therefore, not a relevant process when describing energy spectra. However, the produced secondary muons do not deposit their energy near the interaction point but can propagate longer distances through the detector. In the case of larger transversal momenta of the secondary particles, these multiple muons can be spatially separated from each other, thus producing unique detector signatures. For small transversal momenta, the muon tracks overlap and are therefore indistinguishable. This aspect must be considered, e.g., when analyzing the energy loss behavior of muons and muon bundles. Therefore, muon pair production has been implemented in PROPOSAL, as described in Appendix A.1, using the cross section based on [13]. For electrons and taus, this cross section is not applicable.

The weak interaction describes the interaction of a charged lepton, exchanging a W boson with a nucleus while transforming into a neutrino. This interaction is extremely rare compared to all other processes, as Fig. 1 indicates. However, if a muon undergoes a weak interaction inside a detector, its track will disappear and end in a large hadronic cascade, as the track of the outgoing neutrino is not detectable. Notably, this specific signature might be a background for tau neutrino searches. Therefore, this process has been implemented in PROPOSAL using the cross sections described in Appendix A.2, using the cross section based on [14]. Note that the interaction with the neutral Z boson has not been implemented, as the muon will not disappear, so no significant detector signature is produced.

2.2. New photonuclear parametrizations

Photonuclear interactions have the largest theoretical uncertainties regarding interactions of high-energy muons (≈10%). While this uncertainty is of minor importance for muons around TeV energies, where photonuclear interactions contribute only 10% to the overall energy loss, this contribution increases with the muon energy. At energies above EeV, most energy is lost through photonuclear interactions, as visible in Fig. 1. Therefore, increasing the accuracy of photonuclear interactions is essential to improve high-energy muon propagation.

However, at these energies, the cross sections can not be validated with experimental measurements and depend on the underlying models. Therefore, two further parametrizations have been implemented. The *AbtFT* parametrization [15] fits the model of the ALLM parametrization, the current default cross section, to more recent measurements. The *BlockDurandHa* parametrization [16] has the advantage compared to the ALLM models, that it by design obeys the Froissart bound. Both parametrizations are also applicable for electron or tau propagation. The cross sections of both parametrizations are described in Appendix B, and a visual comparison with the current default cross section of PROPOSAL is shown in Fig. 2.

2.3. Deflection of stochastic interactions

In addition to multiple scattering, i.e., lateral particle displacement during a continuous step, particles can be deflected in individual stochastic (discrete) interactions, as illustrated in Fig. 3. As a distinction to multiple scattering, these processes are called *stochastic deflections* in the following. While multiple scattering is already

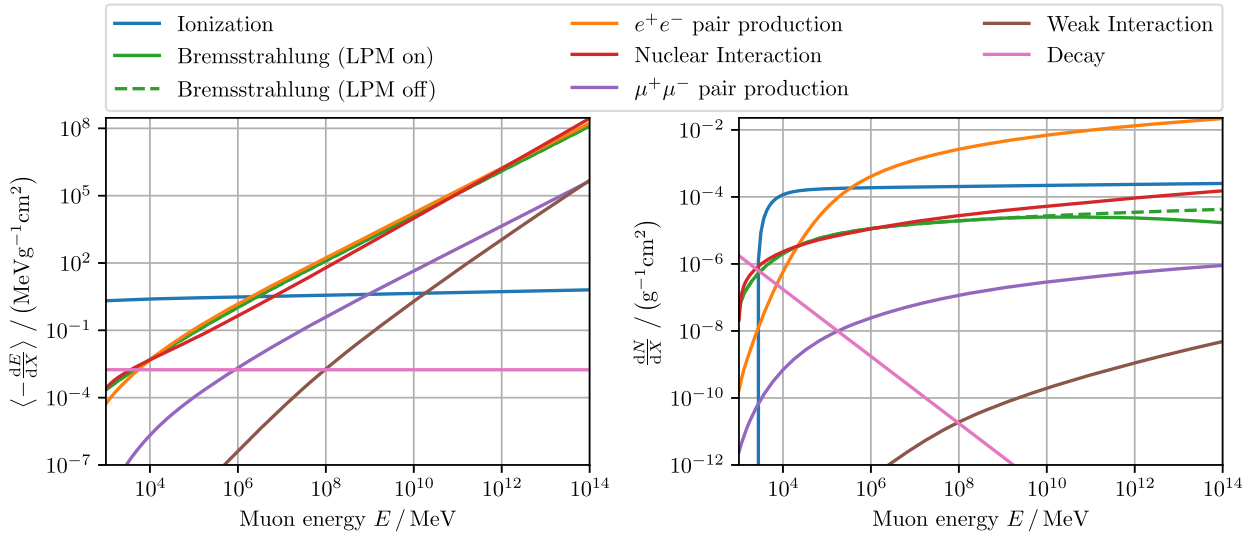

Fig. 1. Muon interactions in ice. The left figure shows the average energy loss per grammage, while the right figure shows the number of stochastic interactions. In this example, interactions with an energy loss above 500 MeV are treated as stochastic. For all interactions, the default parametrizations (see Table G.7) are used.

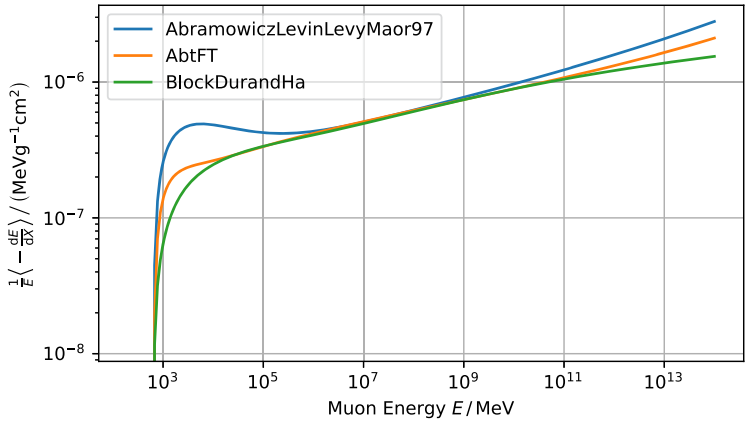

Fig. 2. Comparison of the average muon energy loss in ice due to photonuclear interactions. The two new parametrizations in comparison to the current default cross section in PROPOSAL are shown.

considered inside PROPOSAL, stochastic deflections have so far been neglected since stochastic interactions of high-energy muons are strongly boosted in the forward direction. In order to improve accuracy, stochastic deflections of muons for ionization, electron-positron pair production, bremsstrahlung, and photonuclear interactions have been implemented. For deflections in photonuclear interactions and bremsstrahlung, parametrizations using either the calculation of Van Ginneken [17] or as implemented in GEANT4 [18,19] are provided. The parametrization for electron-positron production is also based on the calculations by Van Ginneken, and the deflection angle due to ionization is directly calculated using conservation of four-momentum. For each parametrization, it is observed that the lower the energy and the larger the energy loss, the larger the deflection. The parametrizations are described in detail in Appendix C, and an overview is presented in Table G.8. Fig. 4 shows the distribution of individual stochastic muon deflections for the different parametrizations and interaction types. For each parametrization, except ionization, deflection angles extend over several orders of magnitude and angles larger than 1° are possible.

During particle propagation, there is not only one interaction but a multitude of individual interactions, depending on the particle energy and the propagation distance. In each interaction, the particle is deflected by an angle θ. All of these single deflections, in addition to the displacement due to multiple scattering, accumulate and lead to a total deflection angle θ_{acc}, which compares the direction of the muon before and after the propagation. A histogram of total deflection angles θ_{acc}, once for particle propagation with and once without stochastic deflections, is presented in Fig. 5. Both distributions agree without a significant difference. However, since large stochastic deflection can occur in individual events, it is necessary to include this effect in simulations, e.g., for experiments reconstructing muon tracks with a high angular resolution. The impact of stochastic deflections and multiple scattering on the directional reconstruction for neutrino telescopes, like the IceCube Neutrino Observatory, are analyzed in detail in [20,21]. In addition, a comparison of the accumulated muon deflection between data and PROPOSAL simulations is shown in [21].

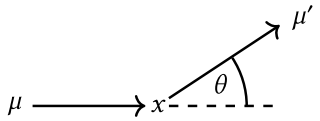

Fig. 3. An incoming muon is deflected by an arbitrary interaction x. The outgoing muon is deflected by the angle θ [20].

To be able to estimate the effect of possible uncertainties in deflection parametrizations, an option to arbitrarily scale stochastic deflection or multiple scattering angles is provided by PROPOSAL. For this purpose, a multiplier ζ, which can be individually set for each interaction type, is applied to the sampled angle by

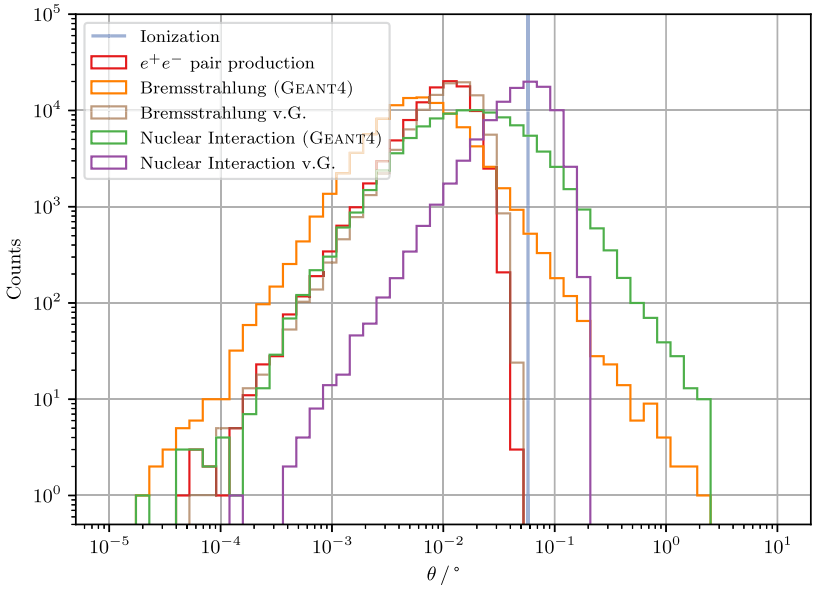

Fig. 4. For all interaction types relevant for muons, 100 000 angles are sampled for each deflection parametrization shown in Fig. C.15. The muon energy is set to 1 TeV, and an energy loss of 50% is applied. Due to different sampling methods between Van Ginneken (v.G.) and GEANT4, outliers to larger deflections are neglected in Van Ginneken, but the most probable angle is shifted to larger values in Van Ginneken. A single deflection can extend over several orders of magnitude for fixed settings.

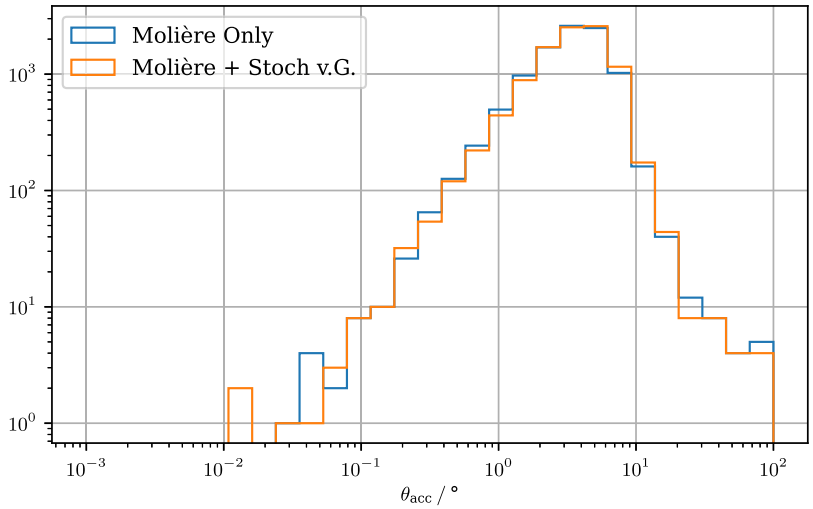

Fig. 5. Accumulated deflection θ_{acc} between the ingoing and outgoing muon direction. In total, 10 000 muons are propagated in ice with an initial energy of 1 TeV to a final muon energy of 1 GeV. A relative energy cut of $v_{cut} = 10^{-3}$ is used. A comparison between the simulation using only multiple scattering, according to Molière, and a simulation using both multiple scattering and stochastic deflections, according to Van Ginneken (v.G.), is shown.

$$\theta_s = \zeta \cdot \theta \,. \tag{1}$$

For multiple scattering, the displacement of the particle relative to the initial axis is scaled.

So far, the deflection parametrizations are only available for muons. Further parametrizations for electrons and positrons need to be implemented in the future.

2.4. Correction of the Landau-Pomeranchuk-Migdal effect

The Landau-Pomeranchuk-Migdal (LPM) effect describes a suppression of small bremsstrahlung losses and pair production processes with a symmetric energy distribution, which is relevant for very-high energies or in dense media. Within the Migdal functions, an energy scale E_{LPM} appears, which can be interpreted as the transition point above which LPM suppression sets in. Different conventions for this quantity exist, which differ by a factor of 8, leading to different formulae for the Migdal functions. In earlier versions, different conventions were mixed, such that the LPM suppression of bremsstrahlung started at too low energies. A careful comparison of the LPM suppression in electron and muon processes with literature [22,23] confirms the correctness of the new implementation. Exemplarily, Fig. 6 shows the effect of these improvements regarding muon energy losses in iron.

3. Implementation of high-energy electron, positron, and photon interactions

Originally, PROPOSAL has been designed for muon and tau propagation in large, homogeneous media. However, the astroparticle physics community needed a modern and modular interaction module that describes all types of electromagnetic particles. Since the description of electron, positron, and photon interactions relies on similar approaches from both a methodological and physical point of view, PROPOSAL has

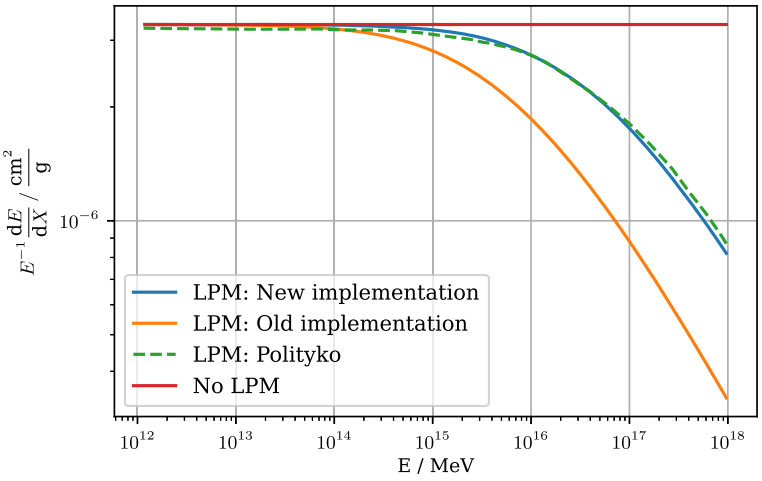

Fig. 6. Average energy loss of muons in iron due to bremsstrahlung, with the LPM effect implementation in the old and new PROPOSAL version. As a validation, calculations from [23] are shown. Without the LPM effect, the old implementation, new implementation, and the calculations from [23] are identical.

been updated to include the necessary parametrizations. This extension allows the library to be used for the physics description of the electromagnetic and muonic component particle cascades, for example, in the air shower simulation framework CORSIKA 8 [24,25].

For electrons and positrons, new parametrizations to describe ionization and bremsstrahlung interactions have been implemented. Furthermore, an adapted parametrization for electron-positron pair production is now available. As it is relevant for positrons at lower energies and essential for describing the charge excess of electrons over positrons, annihilation has been added as a new interaction type. For the description of multiple scattering, photonuclear interactions, weak interaction, and the LPM effect on bremsstrahlung, the parametrizations already available in PROPOSAL can be directly applied for electrons and positrons [1,11]. The details of these parametrizations and their usage in PROPOSAL are described in Appendix D. Fig. 7a shows the average energy loss of positrons in air, using all interaction types available in PROPOSAL. By default, PROPOSAL uses the parametrizations summarized in Appendix G.

For the description of photons, the most crucial interaction types are photoelectric absorption (dominant in air at energies below ≈30 keV), Compton scattering (dominant in air at energies below ≈20 MeV), and electron-positron pair production (dominant at higher energies). Therefore, these interaction types have been implemented in PROPOSAL. In addition, muon pair production and photonuclear interactions have been implemented as additional processes. While their contribution to the mean free path of photons is negligible, they are the processes responsible for the production of hadrons and muons in electromagnetic showers, with photonuclear interaction producing most of the lower energy muons, while muon pair production produces most of the higher energy muons [26]. The photon parametrizations mentioned above and their implementation in PROPOSAL are described in Appendix E. Fig. 7b shows the cross section of photons in air.

The validity of PROPOSAL as an electromagnetic interaction model has been shown by comparing extensive air showers simulated with CORSIKA 8, using PROPOSAL as a model to describe the electromagnetic and muonic shower component, to air showers simulated with established frameworks such as CORSIKA 7, which uses an adapted version of the code EGS4 [28] to describe the electromagnetic shower component [29,30]. For relevant shower parameters such as the longitudinal and lateral shower development, an agreement of 10% or better, depending on the exact simulation settings, can be observed. Furthermore, the simulation of radio signals in air showers shows a good agreement, which is highly dependent on a correct description of the electromagnetic component and, therefore, a sensitive test for PROPOSAL [31].

4. Calculation of secondary particles

Initially, PROPOSAL only calculated the energy losses of particles, characterized by their interaction types, energies, and positions. This update includes the functionality to calculate individual secondary particles out of these energy losses, which is necessary to describe particle cascades. One or several parametrizations to describe this process are provided for each interaction type. Each parametrization defines a `CalculateSecondaries()` method, receiving information about the stochastic energy loss, which can, for example, be obtained from the propagator output as explained in Section 6.6, and returns information about the secondary particles. The technical details of this process are visualized in Fig. 8. Note that the calculation of secondary particles is independent of the propagation, i.e., the sampling of energy losses, and is therefore optional. Accordingly, this feature does not affect the performance of applications where only the energy losses are relevant.

Each parametrization solves two related physical tasks: Calculating the energies and the directions of the secondary particles. The underlying concepts are presented in the following sections.

4.1. Sampling the energy of secondary particles

This task is trivial for interactions with only a single secondary product since the entire energy loss $E \cdot v$ is assigned to the only secondary particle. Those interactions are bremsstrahlung, ionization, Compton scattering, and photoelectric interactions. For interactions with two secondary particles that receive energies E_1 and E_2, where the differential cross section is given in $x = E_1/(E_1 + E_2)$, the energy partition can be sampled by solving the integral equation

$$\frac{1}{\sigma}\int_{x_{\min}}^{x} \frac{\mathrm{d}\sigma}{\mathrm{d}x'}\,\mathrm{d}x' = \xi$$

for x, with a random number $\xi \in [0, 1)$ and the total cross section σ. This approach is used for annihilation, electron-positron pair production, and muon pair production. For electron-positron and muon pair production by leptons, the parametrization is described as a double-differential cross section (see Appendix D.3). However, the utilized approach is identical, with the second variable being fixed.

An extra treatment is necessary for the photonuclear interaction of photons and leptons. The complexity of hadronic interactions, which exceeds the scope of PROPOSAL, requires the usage of external hadronic event generators to sample secondary particles. For hadronic interactions, PROPOSAL returns a pseudo-particle, containing information

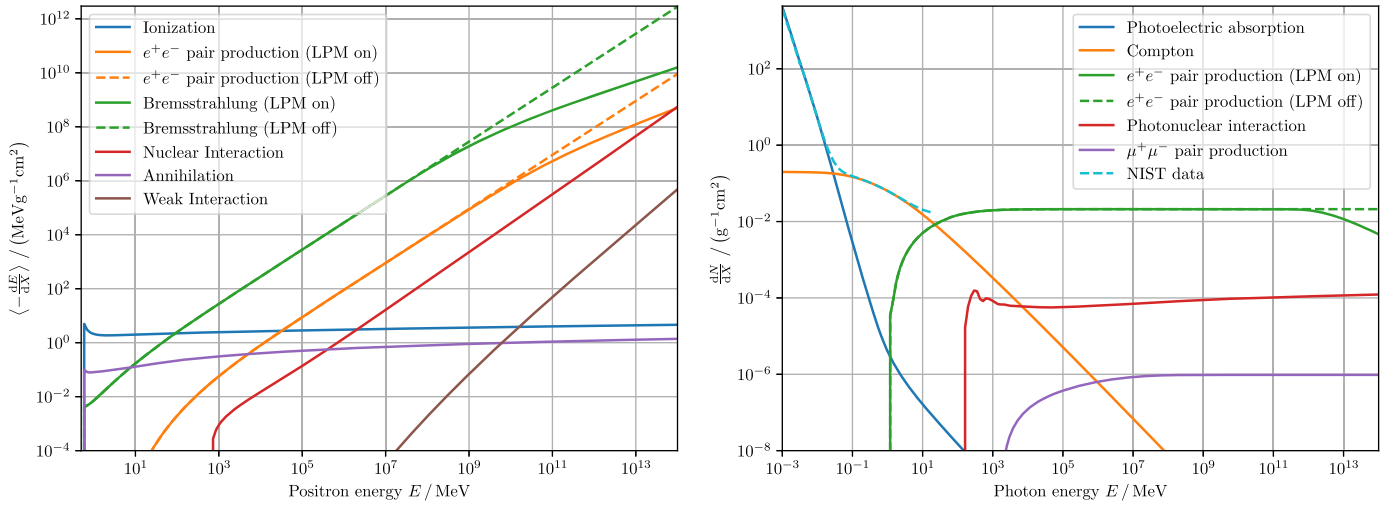

(a) Average positron energy loss per grammage.

(b) Cross section of photons. As a comparison, the photon cross section according to the NIST Standard Reference Database is shown [27].

Fig. 7. Cross sections of positron and photon ([27]) interactions in air, described by the default parametrizations given in Appendix G.

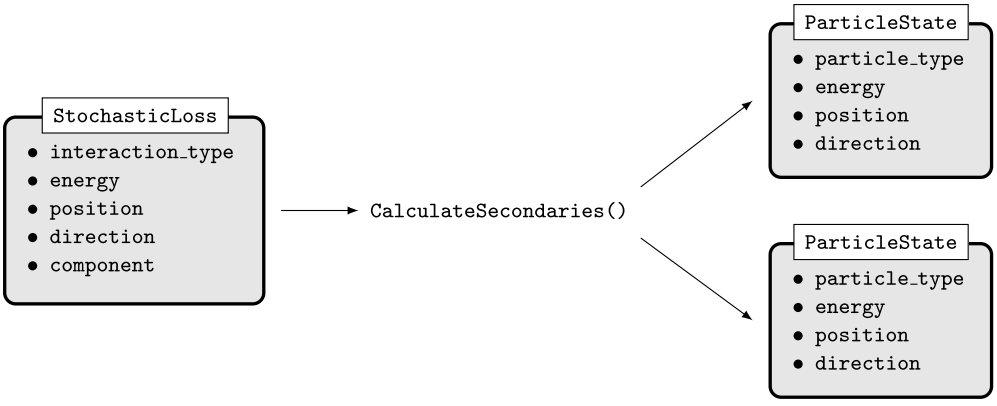

Fig. 8. Visualization of the `CalculateSecondaries()` method. As an input, the method receives a `StochasticLoss` object, characterizing the stochastic energy loss of the parent particle. The output is a list of `ParticleState` objects, where each object describes the properties of a produced secondary particle. Note that the number of created `ParticleState` objects can be different. In this example, two secondary particles are created.

about the energy lost in the interaction and the identity of the interaction target. The user can process this information outside of PROPOSAL by passing it to a hadronic event generator. This approach is, for example, implemented in the air shower simulation framework CORSIKA 8 [25], where for hadronic energy losses, the information provided by the pseudo-particle is passed to Sibyll [32] or SOPHIA [33], depending on the chosen transition energy between the low and high-energy hadronic interaction model [30]. The accuracy of this approach is defined by the validity of the underlying photohadronic cross section, provided by PROPOSAL, and the assumptions made by the used hadronic interaction model. For a more consistent treatment, a sampling of the transferred momentum for cross sections that are differential in Q^2 could be implemented in a future update.

4.2. Sampling the direction of secondary particles

For interactions that can be approximated as a two-body interaction with an atomic electron at rest, assuming both energy and momentum conservation, the polar angles of the secondary particles can be calculated deterministically. In this case, only the energies of the secondary particles need to be known. This approximation is used for ionization, annihilation, and Compton scattering. The azimuth angle is sampled uniformly for one secondary particle between 0 and 2π, with the other particle receiving the opposite azimuth.

For electron-positron pair production and the photoelectric effect, the assumption that the secondary particles inherit the direction of the parent particle is made. A more sophisticated description might be added in a future update.

Since bremsstrahlung and electron-positron pair production are the predominant processes for high-energy electromagnetic cascades, their precise treatment is of particular importance. As a first approximation, the assumption of a polar angle $\theta = m_e/E_0$ can be used, where E_0 denotes the energy of the initial particle. It is possible to use such a simple description since for high energies, the particle production is strongly peaked towards the forward direction, while for lower energies, multiple scattering effects dominate the lateral behavior of the electromagnetic cascade [28].

As an alternative, a rejection sampling method for the bremsstrahlung angle distribution, based on the double differential cross section by Koch and Motz [34], has been implemented. The details of this method are described in Appendix F.1. Fig. 9a compares both approaches to sample the production angle of bremsstrahlung photons. The direction of the outgoing electron or positron is calculated assuming momentum

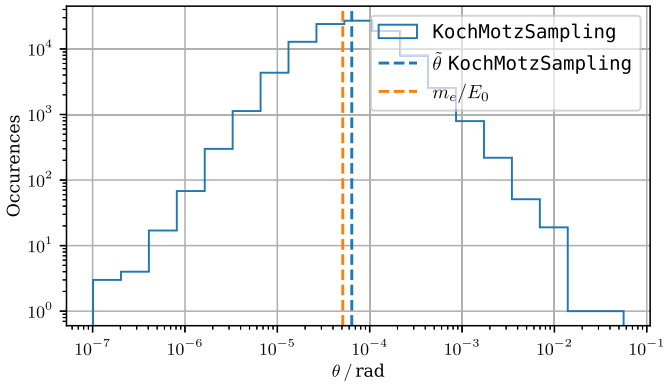

(a) Production angles of bremsstrahlung photons created by electrons or positrons. The plot shows a comparison of the $\theta = m_e/E_0$ approximation with the parametrization `KochMotzSampling`, described in Appendix F.1.

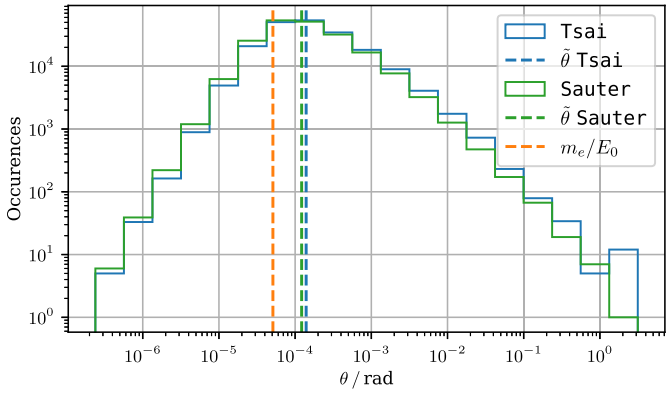

(b) Production angles of electron and positrons created by photons. Compared are the $\theta = m_e/E_0$ approximation , the `Tsai` parametrization according to (F.7), and the `Sauter` sampling procedure according to (F.9).

Fig. 9. Production angles of secondary particles in air, with an initial particle energy of $E = 10^4$ MeV. The variable $\tilde{\theta}$ indicates the median of the corresponding distribution.

conservation and neglecting the momentum transferred to the nucleus in the bremsstrahlung interaction.

For electron-positron pair production, two additional alternatives to the $\theta = m_e/E_0$ approximation have been implemented. These methods are based on differential cross sections describing the angular distribution of the produced leptons. The first method, `Tsai`, is based on the parametrization described in [35], while the second method, `Sauter`, is based on a parametrization given in [36]. Both methods are described in Appendix F.2. Fig. 9b compares all three sampling approaches.

An analysis of the development of electromagnetic particle showers described with PROPOSAL is presented in the context of air shower simulations with CORSIKA 8 in [30,29]. Comparisons with CORSIKA 7, where the electromagnetic shower component is described by EGS4, reveal an agreement within 5% for the longitudinal and lateral shower development.

5. Propagation in media with inhomogeneous densities

This update introduces the possibility of propagating particles through inhomogeneous density distributions, allowing for a more detailed description of the environment, for example, the overburden of underground experiments or the atmosphere of the Earth. This depicts an improvement in both performance and precision compared to the alternative approach, where inhomogeneous media need to be approximated via individual layers with constant density. To make this possible, cross sections and the corresponding interaction integrals are now internally calculated in terms of grammage[1] instead of distances, making them independent of the actual density distribution. Assuming the density is a linear factor in the cross section, the density correction can be separated from the average energy loss, i.e.

$$f(E) := \frac{\mathrm{d}E}{\mathrm{d}X} = \frac{\mathrm{d}E}{\mathrm{d}x}\frac{1}{\rho(x)}. \tag{2}$$

This integral can be solved by separation of variables

$$\int \frac{1}{f(E)}\mathrm{d}E = \int \rho(x)\mathrm{d}x, \tag{3}$$

describing the relation between energies and distances given a density distribution $\rho(x)$. Four different options to describe $\rho(x)$ have been implemented: A homogeneous distribution, an exponential distribution, a polynomial distribution, and the description of the distribution via splines. The density inside a geometry can be varied along a Cartesian or a radial axis. For a given origin $\vec{f}_{p_0}$, the depth $d(\vec{x})$ of a radial axis is calculated by

$$d(\vec{x}) = |\vec{x} - \vec{f}_{p_0}|. \tag{4}$$

For a Cartesian axis, an additional direction $\vec{f}_{\text{axis}}$ needs to be defined, and $d(\vec{x})$ is calculated by

$$d(\vec{x}) = \vec{f}_{\text{axis}} \cdot (\vec{x} - \vec{f}_{p_0}). \tag{5}$$

The exponential distribution is then defined by the scaling parameter σ and the shifting parameter d_0, resulting in the density profile

$$\rho(\vec{x}) = \rho_0 \cdot \exp\left(\frac{d(\vec{x}) - d_0}{\sigma}\right). \tag{6}$$

The polynomial distribution is described by the coefficients a_k, resulting in the density profile

$$\rho(x) = \rho_0 \cdot \sum_{k=0}^{n} a_k d(x)^k. \tag{7}$$

Either a linear or a cubic spline interpolation can be used to describe the spline density profile.

Treating the density correction as a linear factor as assumed in (2) is not valid when the LPM effect (see Section 2.4) is taken into account, which contains a non-linear density dependency. However, creating density-independent interpolation tables of the cross sections and propagation integrals requires this assumption. Therefore, the LPM effect can only be considered using a reference point with a fixed density, assuming no significant density changes. Since the density effects are mainly minor corrections or have significant effects only at higher energies, this approximation is still valid for most environments. However, this issue needs to be addressed in a future update, especially in the context of electron, positron, and photon propagation in the atmosphere.

6. Technical improvements

6.1. Installation process

The current dependencies of PROPOSAL are the libraries `cubic_interpolation` [37], `spdlog` [38], `nlohmann_json` [39], and

[1] Grammage describes the density integrated over a distance x, i.e. $X = \int \rho(x)\,\mathrm{d}x$, with the density distribution $\rho(x)$ along the particle trajectory.

pybind11 [40], where the latter is only necessary if python bindings are supposed to be created. The installation of PROPOSAL is based on CMake. Instead of manually providing all dependencies, they can be provided by the C++ software package manager conan [41]. Installation of PROPOSAL as a C++ library using conan works via the commands:

```
$ pip install conan
$ git clone \
$ https://github.com/tudo-astroparticlephysics/
  PROPOSAL.git
$ cd PROPOSAL
$ conan install . --build=missing
$ cd build
$ cmake .. -DCMAKE_TOOLCHAIN_FILE=conan_toolchain.
  cmake
$ cmake --build . -j
$ cmake --install .
```

The step `conan install` provides the dependencies by either fetching their binaries or building them, which are then passed to CMake, which is used to build and install PROPOSAL in the usual way.

For the usage of PROPOSAL as a Python package, versions later than `v6.1.0` can be installed via the Python software repository PyPi [42], with the command:

```
$ pip install proposal
```

In addition to Linux and macOS, PROPOSAL is now also developed and tested for Windows. A detailed description of the installation process is provided in https://github.com/tudo-astroparticlephysics/PROPOSAL/blob/master/INSTALL.md.

6.2. Modularization

As a central feature, PROPOSAL provides a complete three-dimensional Monte Carlo simulation of individual particles. Given an input, where the initial particle state and the propagation environment are defined, PROPOSAL returns information about the energy losses and particle states, where the output is explained in detail in Section 6.6. This functionality is provided by the `Propagator` class.

Several calculations regarding the continuous and stochastic (discrete) interaction have to be performed to execute a propagation step. For this update of PROPOSAL, these tasks have been moved from inside the `Propagator` class to individual modules, which are used by the `Propagator` but can also be used as standalone classes. This restructuring allows PROPOSAL to be used also as a modular library. Six different modules are available: The *Interaction*, *Decay*, *ContinuousRandomization*, *Displacement*, *Time*, and *Scattering* module. [43]

The *Interaction* module provides the method to calculate the energy E_f of the next stochastic interaction, which is defined as an interaction with a relative energy loss above a selected energy cut v_cut. To calculate E_f, the integral equation

$$\int_{E_\mathrm{i}}^{E_\mathrm{f}} \frac{\sigma(E)}{-f(E)}\,\mathrm{d}E = -\log\xi \tag{8}$$

is solved, where $\sigma(E)$ is the total stochastic cross section, $f(E) = \mathrm{d}E/\mathrm{d}X$ the average energy loss per grammage, and $\xi \in [0,1)$ a random number [1]. Furthermore, the type and size of a stochastic energy loss can be sampled from the differential cross section. Lastly, the individual integrated cross sections of the different processes and their sum can be accessed. With the *Decay* module, the final energy for which the particle will decay is sampled, given the particle's lifetime and current energy. The *ContinuousRandomization* module provides a Gaussian smearing of the continuous energy loss, where the mean of the smearing is calculated according to

$$\left\langle \Delta(\Delta E)^2 \right\rangle = \int_{E_\mathrm{i}}^{E_\mathrm{f}} \frac{E^2}{-f(E)} \left\langle \frac{\mathrm{d}^2 E}{\mathrm{d}X^2} \right\rangle. \tag{9}$$

This method can resolve simulation artifacts, which can occur when using large energy cuts [1]. The time elapsed during a propagation step can be calculated with the *Time* module using

$$t_\mathrm{f} = t_\mathrm{i} + \int_{x_\mathrm{i}}^{x_\mathrm{f}} \frac{\mathrm{d}x}{v(x)} = t_i - \int_{E_i}^{E_f} \frac{\mathrm{d}E}{f(E)v(E)}, \tag{10}$$

while the grammage covered during a propagation step with a given initial and final energy is calculated by

$$X_\mathrm{f} = X_\mathrm{i} - \int_{E_\mathrm{i}}^{E_\mathrm{f}} \frac{\mathrm{d}E}{f(E)}, \tag{11}$$

which is provided by the *Displacement* module. Additionally, this module calculates the final energy for a given initial energy and grammage, which is the inversion of the integral in (11). Lastly, the *Scattering* module is responsible for describing the lateral particle development. For the displacement during a continuous propagation step, multiple scattering, using the methods described in Section 6.4, can be applied [11]. The particle deflection during a stochastic interaction is also calculated here, according to the methods described in Section 2.3.

One application example of this modular structure is the particle cascade framework CORSIKA 8, which uses the modules provided by PROPOSAL to calculate the electromagnetic and muonic shower component of extensive air showers [24,25,29]. Here, CORSIKA 8 provides the overall algorithm for the Cascade simulation, resorting to physics information from PROPOSAL, for example the mean free path length or the sampling of stochastic interactions (provided by the *Interaction* module), conversions of covered grammages to particle energies and vice versa (provided by the *Displacement* module), or the description of multiple scattering (provided by the *Scattering* module).

6.3. Improved interpolation routine

Several numerically-expensive evaluations of one or two-dimensional integrals are performed during the propagation process. To speed up this process, PROPOSAL uses interpolation tables to store the results of these integrations. Previous versions of PROPOSAL used a self-implemented polynomial and rational interpolation routine [1]. However, this implementation could show an unstable behavior for functions with non-differentiable parts caused by features present within physics parametrizations or artifacts introduced by the energy cuts. The upper part of Fig. 10 shows an example of this behavior.

This update of PROPOSAL uses the `cubic_interpolation` [37] library for interpolations. It provides an implementation of one-dimensional cubic interpolation and two-dimensional bicubic interpolation, based on the Eigen library [44] and the `cardinal_cubic_b_spline` class from the Boost.Math library [45]. Furthermore, linear and exponential axis transformations and methods to solve integral equations are available.

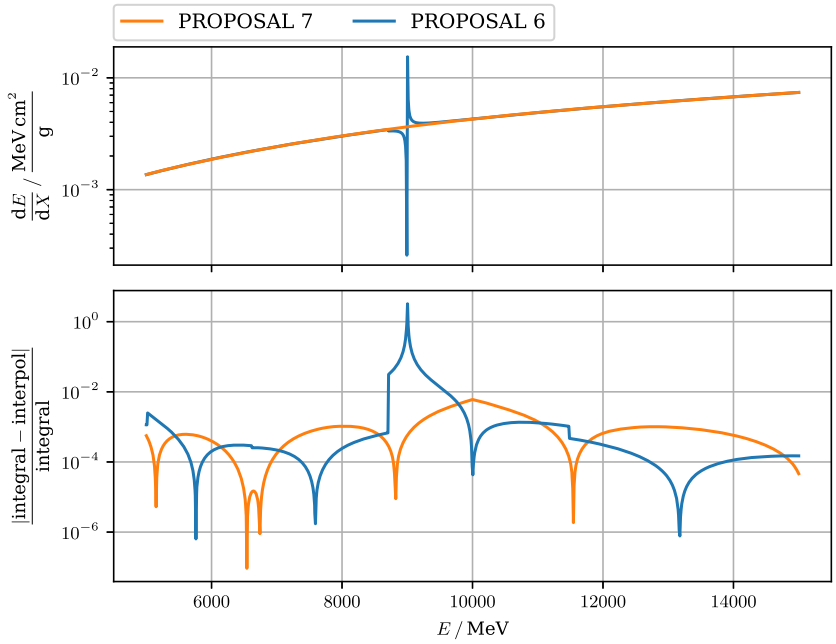

Fig. 10. Comparison of the interpolation routine used in PROPOSAL 6 and PROPOSAL 7. Exemplarily, the average pair production energy loss of a muon in ice, using an energy cut of $E_{\text{cut}} = 500$ MeV, $v_{\text{cut}} = 0.05$, is shown. The upper plot shows the absolute value of the interpolation, the lower plot the ratio between integration and interpolation for PROPOSAL 6 and PROPOSAL 7. Note that for a fair comparison, the number of interpolation nodes has been set to 100 in both PROPOSAL versions. By default, PROPOSAL 7 uses a higher number of interpolation notes to achieve a better precision.

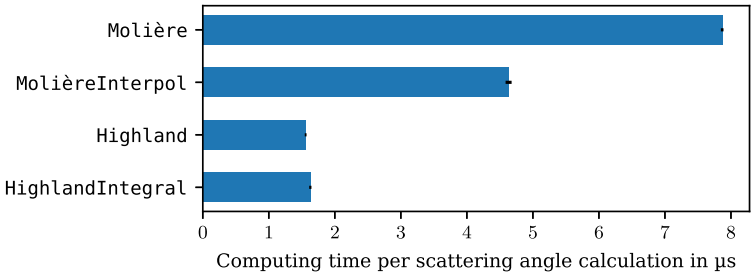

Fig. 11. Comparison of the average runtime to calculate a scattering angle according to the different parametrizations implemented in PROPOSAL. A statistic of 10^7 samples is used.

Fig. 10 compares the performance of the interpolation routines of PROPOSAL 6 and PROPOSAL 7 for a function with a non-differentiable behavior. Note that while the interpolation routine of PROPOSAL 6 shows an unphysical artifact, the interpolation in PROPOSAL 7 remains at a stable accuracy.

6.4. Runtime improvements for multiple scattering

To describe multiple scattering, different parametrizations to sample the deflection angles are available. The most accurate description is given by the `Molière` parametrization, while the `Highland` and `HighlandIntegral` parametrizations are a Gaussian approximation of `Molière` [11]. While they provide an incomplete description of outliers, i.e., large scattering angles, the parametrizations of `Highland` and `HighlandIntegral` are much quicker to evaluate, as can be seen in Fig. 11. However, for some applications, the more accurate description of `Molière` is necessary, for example, to describe the scattering of electrons and positrons at low energies. To improve the computing time, the evaluation of two series expansions, which were previously calculated using Horner's method, have been replaced by two interpolation tables. This method, called `MolièreInterpol`, improves the overall evaluation time of the scattering angles by a factor of ≈ 2, as shown in Fig. 11, while providing the same results.

6.5. Restructuring of the propagation algorithm

With this update of PROPOSAL, the propagation algorithm has been restructured, introducing a more intuitive and consistent structure, also considering the inclusion of non-decaying particles.

A propagation step is either limited by a process that occurs at a given particle energy E_{limit}, or by a process that occurs after a given distance x_{limit}. To find the process that limits the propagation step, the following approach is used:

Firstly, the limiting energy is determined by

$$E_{\text{limit}} = \max(E_{\text{interaction}}, E_{\text{decay}}, E_{\text{min}}), \tag{12}$$

where $E_{\text{interaction}}$ is the energy where the next stochastic energy loss would occur (taking into account all possible energy loss processes), sampled according to (8); E_{decay} is the energy where the particle would decay; and E_{min} is a given lower energy threshold where the particle is forced to stop. The threshold E_{min} is a new feature of PROPOSAL which can optionally be defined when propagating a particle. The determined value of E_{limit} is converted to a distance $x_{\text{limit,E}}$ by solving (11) with $E_f = E_{\text{limit}}$.

Next, the limiting distance is determined by

$$x_{\text{limit}} = \min(x_{\text{max}}, x_{\text{border}}), \tag{13}$$

Table 1
Methods provided by the `Secondaries` class, providing access to the output information of a propagation process.

Method	Method description
`GetStochasticLosses()`	Returns list of all stochastic losses during propagation.
`GetStochasticLosses(geometry)`	Returns list of all stochastic losses inside a geometry.
`GetStochasticLosses(type)`	Returns list of all stochastic losses of a given interaction type.
`GetContinuousLosses()`	Returns list of all continuous losses during propagation.
`GetContinuousLosses(geometry)`	Returns list of all continuous losses inside a geometry.
`GetInitialState()`	Particle state at start of propagation.
`GetFinalState()`	Particle state at the end of propagation.
`GetStateForEnergy(energy)`	Particle state for a given energy.
`GetStateForDistance(distance)`	Particle state for a given propagation distance.
`GetEntryPoint(geometry)`	Return particle state when entering geometry, if applicable.
`GetExitPoint(geometry)`	Return particle state when leaving geometry, if applicable.
`GetClosestApproachPoint(geometry)`	Return particle state when the smallest distance to the center of geometry has been reached.
`HitGeometry(geometry)`	Returns true if a geometry has been hit.
`GetELost(geometry)`	Returns sum of energy that has been deposited in geometry.
`GetDecayProducts()`	Returns list of decay products, if particle has decayed at the end of propagation.

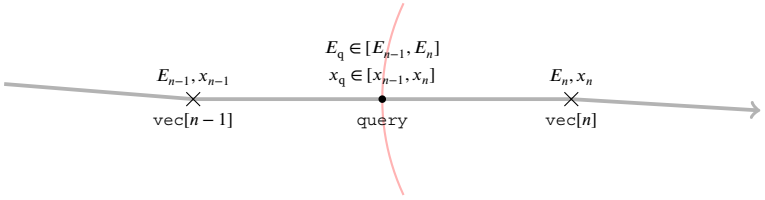

Fig. 12. Visualization of the concept to calculate particle states at arbitrary query points, given the stored particle states `vec` with the corresponding particle energies E_n and propagated distances x_n. Note that the particle track is assumed to be the direct connection of the stored particle positions. In this example, the query position is defined by the intersection of the particle track with a geometry, indicated by the red circular arc. (For interpretation of the colors in the figure(s), the reader is referred to the web version of this article.)

where x_{border} is the distance to the next geometry border, and $x_{\max}$ is the maximal propagation distance at which the particle is forced to stop.

For $x_{\text{limit,E}} < x_{\text{limit}}$, the propagation step is given by the step size $x_{\text{limit,E}}$ and final energy E_{limit}. In case of $E_{\text{limit}} = E_{\text{interaction}}$, the propagation step is followed by a stochastic energy loss, while for $E_{\text{limit}} = E_{\text{decay}}$, the particle decays after the propagation step. For $x_{\text{limit,E}} \geq x_{\text{limit}}$, the propagation step is instead given by the step size x_{limit}, while the final energy is calculated by solving (11) for E_{f} given x_{limit}.

6.6. Revised output of propagator class

This update of PROPOSAL features an improved interface to the output of a particle propagation process. During propagation, the `Propagator` class stores the information about the particle state (i.e., energy, position, direction, time, propagated distance, and most recent interaction type) before and after every stochastic interaction, as well as at sector transitions (which are described in Section 6.7). All particle states are collected in a standard vector. In addition to directly accessing this vector, PROPOSAL now provides query methods to intuitively extract specific information about the propagation output. This includes methods to return lists of all stochastic or continuous energy losses, either in general, for a specific interaction type, or inside a given geometry. Table 1 lists all query methods provided by the `Secondaries` class.

In addition, the particle state at the exit, entry, or closest approach point of an arbitrary geometry can be obtained. The underlying algorithm that is used by PROPOSAL is described as follows: As illustrated in Fig. 12, the algorithm calculates the intersection of the geometry with the particle track, which is given by the direct connection of the positions of the stored particle states. Then, the closest particle state before the intersection point `vec`$[n-1]$, with known energy E_{n-1}, is determined. In addition, the propagated distance of this state, x_{n-1}, and the propagated distance of the intersection, x_{q}, are known, which is sufficient to calculate the particle state at the intersection point. For example, the energy at the intersection point E_q can be calculated by solving the integral equation (11) for $E_{\text{f}} = E_{\text{q}}$, with the already known quantities $x_{\text{f}} = x_{\text{q}}$, $x_{\text{i}} = x_{n-1}$, and $E_{\text{i}} = E_{n-1}$. For the conversions of x to X, i.e., from distances to grammage and vice versa, the underlying density profile needs to be considered (see Section 5). The same approach can be used to request the particle state for an arbitrary propagation distance or particle energy, using (11).

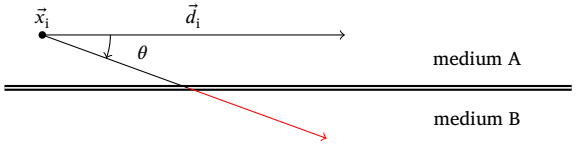

Fig. 13. Visualization of the border transition problem. A particle at position $\vec{x}_{\text{i}}$ within medium A is transferred along an initial direction $\vec{d}_{\text{i}}$. Due to multiple scattering, the initial direction is changed by an angle θ. This can cause the particle to enter a medium B. If this is not correctly taken into account, the particle will traverse a distance through medium B, indicated by the red color, while the algorithm assumes that the particle is still in medium A.

Note that the calculation of the individual decay products is only performed if explicitly requested by the user using the `GetDecayProducts()` method, similar to the calculation of the secondary particles of an interaction described in Section 4. Otherwise, only the decay point is calculated, saving computational resources. This approach also allows users to sample decay products with other, more sophisticated algorithms, for example, the framework `TAUOLA` [46].

6.7. Treatment of border transitions in the propagator

By design, particles simulated with PROPOSAL are allowed to perform large propagation steps. Since calculations provide different results if the underlying medium is different, the borders between sectors pose an upper limit for propagation steps. In previous versions of PROPOSAL, during a propagation step, the particle translation due to multiple scattering has been applied after the energy and distance of the step have been calculated. For particles traveling close to a sector transition, this could lead to problems, as illustrated in Fig. 13. Due to multiple

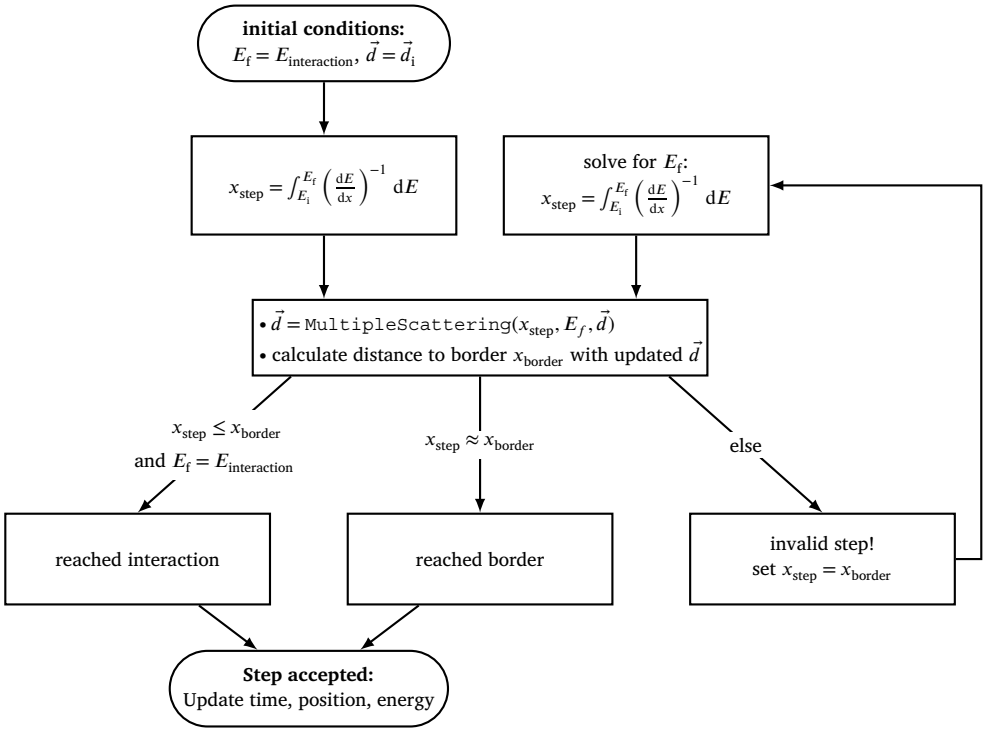

Fig. 14. Flowchart explaining the `AdvanceParticle` method of the `Propagator` class, handling multiple scattering in combination with border transitions. Note that the flowchart shows a simplified version of the algorithm, neglecting special cases such as limitations due to maximal propagation distances or minimal particle energies given by the user (see Section 6.5).

scattering, particles could enter sectors with other medium properties without this being taken into account by the propagation algorithm. Especially for particles traveling in parallel to a sector border and for medium transitions with drastic mass density changes, this could lead to under- or overestimation of energy losses and propagation distances.

A naive solution to this problem would be to re-evaluate the distance to the next border transition after calculating the multiple scattering translation and shorten the propagation step if a border transition is violated. However, since the calculation of the multiple scattering translation is correlated with the distance of a propagation step, this approach would cause an overestimation of multiple scattering.

Therefore, an iterative approach to determine a valid combination of propagation step length and multiple scattering angles has been implemented as illustrated in a simplified version in Fig. 14. Instead of cutting the propagation step according to the updated distance to the border transition, the algorithm recalculates the multiple scattering translation using the updated distance. This calculation is repeated until the difference between the propagation step and the distance to the border transition is within a given precision (by default 10^{-3} cm). In most cases, this algorithm converges after a few iterations.

7. Summary

PROPOSAL is now a complete electromagnetic propagation module for high-energy charged leptons and photons, providing state-of-the-art parametrizations to sample energy losses and deflections. New parametrizations and interaction types have been implemented to enable the propagation of electrons, positrons, and high-energy photons. Instead of simply calculating the energy losses of the propagating particle, the option to calculate individual secondary particles, which can be further propagated, is now available. Muon pair production and weak interactions have been implemented as muon interaction processes, allowing for a better estimation of rare event signatures. Furthermore, model uncertainties concerning the photonuclear interaction can be better quantified due to a larger selection of interaction parameterizations. Next to the physics-related improvements, numerous technical improvements have been made, ranging from more advanced interpolation methods, bug fixes, changes in the propagation routine and output, and an improved installation process, which makes PROPOSAL more user-friendly and flexible to use.

CRediT authorship contribution statement

Jean-Marco Alameddine: Writing – review & editing, Writing – original draft, Visualization, Validation, Software, Methodology, Data curation. **Johannes Albrecht:** Writing – review & editing, Methodology, Funding acquisition. **Hans Dembinski:** Writing – review & editing, Methodology. **Pascal Gutjahr:** Writing – review & editing, Writing – original draft, Visualization, Validation, Software, Methodology, Data curation. **Karl-Heinz Kampert:** Writing – review & editing, Methodology, Funding acquisition. **Wolfgang Rhode:** Writing – review & editing, Supervision, Project administration, Methodology, Funding acquisition, Conceptualization. **Maximilian Sackel:** Writing – review & editing, Validation, Software, Methodology, Data curation. **Alexander Sandrock:** Writing – review & editing, Writing – original draft, Visualization, Validation, Software, Methodology, Data curation. **Jan Soedingrekso:** Writing – review & editing, Writing – original draft, Visualization, Validation, Software, Methodology, Data curation.

Declaration of competing interest

The authors declare that they have no known competing financial interests or personal relationships that could have appeared to influence the work reported in this paper.

Data availability

No data was used for the research described in the article.

Acknowledgements

This work was supported by the *Deutsche Forschungsgemeinschaft* (DFG Collaborative Research Center SFB 1491/F3/F4), the *Bundesministerium für Bildung und Forschung* under the Grand numbers 05A20PEA and 05A23PEA, and the *Lamarr Institute*. The authors thank the CORSIKA 8 collaboration for useful discussions. We are grateful to Maximilian Linhoff for his technical expertise and support in maintaining PROPOSAL.

Appendix A. Rare muon interactions

A.1. Muon pair production by high-energy muons

The parametrization for muon pair production implemented in PROPOSAL is taken from [13]. The cross section is given by

$$\frac{\mathrm{d}\sigma(E,v,\rho)}{\mathrm{d}v\,\mathrm{d}\rho} = \frac{2}{3\pi}\left(Z\alpha r_e \frac{m_e}{m_\mu}\right)^2 \frac{1-v}{v}\Phi(v,\rho)\ln X\,, \tag{A.1}$$

with the relative energy loss $v = (E_{\mu^+} + E_{\mu^-})/E$, the asymmetry parameter $\rho = (E_{\mu^+} - E_{\mu^-})/(E_{\mu^+} + E_{\mu^-})$, and the definition

$$\begin{aligned}\Phi(v,\rho) = {} & [(2+\rho^2)(1+\beta) + \xi(3+\rho^2)]\ln\left(1+\frac{1}{\xi}\right) \\ & + \left[(1+\rho^2)\left(1+\frac{3}{2}\beta\right) - \frac{1}{\xi}(1+2\beta)(1-\rho^2)\right]\ln(1+\xi) \\ & - 1 - 3\rho^2 + \beta(1-2\rho^2)\end{aligned} \tag{A.2}$$

with

$$\beta = v^2/[2(1-v)], \qquad X = 1 + U(E,v,\rho) - U(E,v,\rho_{\max}), \tag{A.3}$$

$$\xi = v^2(1-\rho^2)/[4(1-v)], \qquad \rho_{\max} = 1 - 2m_\mu/(vE), \tag{A.4}$$

with

$$U(E,v,\rho) = \frac{0.65A^{-0.27}BZ^{-1/3}m_\mu/m_e}{1 + \frac{2\sqrt{e}m_\mu^2 BZ^{-1/3}(1+\xi)(1+Y)}{m_e E v(1-\rho^2)}}, \tag{A.5}$$

and

$$Y = 12\sqrt{m_\mu/E}, \qquad B = 183. \tag{A.6}$$

A.2. Weak interaction

For the weak interaction of a charged lepton with a nucleus, the cross sections for neutrinos interacting with a nucleus can be used due to crossing symmetry. Thereby, the neutrino cross section calculated by [14], data of the HERA experiment,[2] were interpolated for an energy range of 10 GeV to 10^{12} GeV. The differential cross sections were tabulated for the proton and neutron cross section. The resulting cross section for PROPOSAL is averaged according to the number of individual nucleons in the nucleus

$$\frac{\mathrm{d}\sigma}{\mathrm{d}y} = \frac{Z}{A}\frac{\mathrm{d}\sigma_\mathrm{p}}{\mathrm{d}y} + \left(1-\frac{Z}{A}\right)\frac{\mathrm{d}\sigma_\mathrm{n}}{\mathrm{d}y}. \tag{A.7}$$

Compared to most other interactions implemented in PROPOSAL, this purely stochastic interaction has no contribution to the continuous energy loss, and the cross section is differential in the Bjorken y, which describes the relative energy transferred to the nucleus. The limits for the Bjorken y in this parametrization are

$$y_{\min} = \frac{Q^2_{\min}}{E(m_\mathrm{p}+m_\mathrm{n}) + \left(\frac{m_\mathrm{p}+m_\mathrm{n}}{2}\right)^2} \qquad \text{and} \qquad y_{\max} = 1, \tag{A.8}$$

where the neutrino mass is neglected for the upper limit, and $Q^2_{\min}$ is set to 1 GeV^2.

[2] For the parton distribution functions, HERAPDF1.5 [47,48] was used.

Appendix B. New photonuclear parametrizations

The `AbtFT` parametrization [15] is a refit of the ALLM parametrization [49] to the combined HERA data [50] in addition to fixed-target data [51–53]. It uses the same formulae as [49], but with the parameters given in Table B.2.

The `BlockDurandHa` parametrization was developed in [16] based on the idea of a saturated Froissart bound. In this model, the structure function F_2 is parametrized as

$$\begin{aligned}F_2(x,Q^2) = {} & D(Q^2)(1-x)^n \\ & \times \left[C(Q^2) + A(Q^2)\ln\left(\frac{Q^2/x}{Q^2+\mu^2}\right) + B(Q^2)\ln^2\left(\frac{Q^2/x}{Q^2+\mu^2}\right)\right],\end{aligned} \tag{B.1}$$

with the squared four-momentum transfer Q^2 and the Bjorken scaling variable x, where

$$A(Q^2) = a_0 + a_1\ln\left(1+\frac{Q^2}{\mu^2}\right) + a_2\ln^2\left(1+\frac{Q^2}{\mu^2}\right), \tag{B.2}$$

$$B(Q^2) = b_0 + b_1\ln\left(1+\frac{Q^2}{\mu^2}\right) + b_2\ln^2\left(1+\frac{Q^2}{\mu^2}\right), \tag{B.3}$$

$$C(Q^2) = c_0 + c_1\ln\left(1+\frac{Q^2}{\mu^2}\right), \tag{B.4}$$

$$D(Q^2) = \frac{Q^2(Q^2+\lambda M^2)}{(Q^2+M^2)^2}. \tag{B.5}$$

The values of the parameters determined from the real photoabsorption cross section parametrization by [54] and combined HERA data [47] are given in Table B.3.

Table B.2
Values of the parameters of the ALLM parametrization from the HHT-ALLM-FT fit in [15].

Parameter	Value	Parameter	Value
$a_1^{\mathbb{P}}$	−0.075	$a_1^{\mathbb{R}}$	0.882
$a_2^{\mathbb{P}}$	−0.470	$a_2^{\mathbb{R}}$	0.082
$a_3^{\mathbb{P}}$	9.2	$a_3^{\mathbb{R}}$	−8.5
$b_1^{\mathbb{P}}$	−0.477	$b_1^{\mathbb{R}}$	0.339
$b_2^{\mathbb{P}}$	54.0	$b_2^{\mathbb{R}}$	3.38
$b_3^{\mathbb{P}}$	0.073	$b_3^{\mathbb{R}}$	1.07
$c_1^{\mathbb{P}}$	0.356	$c_1^{\mathbb{R}}$	−0.636
$c_2^{\mathbb{P}}$	0.171	$c_2^{\mathbb{R}}$	3.37
$c_3^{\mathbb{P}}$	18.6	$c_3^{\mathbb{R}}$	−0.660
m_0^2	0.338 GeV^2	$m_{\mathbb{R}}^2$	0.838 GeV^2
Λ^2	4.4×10^{-9} GeV^2	$m_{\mathbb{P}}^2$	50.8 GeV^2
Q_0^2	1.87×10^{-5} GeV^2		

Table B.3
Fit values of the `BlockDurandHa` parametrization from [16].

Parameter	Value	Parameter	Value
a_0	8.205×10^{-4}	c_0	0.255
a_1	-5.148×10^{-2}	c_1	1.475×10^{-1}
a_2	-4.725×10^{-3}	n	11.49
b_0	2.217×10^{-3}	λ	2.430
b_1	1.244×10^{-2}	M^2	0.753 GeV^2
b_2	5.958×10^{-4}	μ^2	2.82 GeV^2

Appendix C. Deflection parametrizations

The following parametrizations by Van Ginneken [17] have been validated for energies 3 GeV $< E <$ 30 TeV. A relative energy loss v_{loss} is introduced as

$$v_{\text{loss}} = \frac{E_{\text{loss}}}{E}, \tag{C.1}$$

with the absolute energy loss E_{loss}, the initial muon energy E, and

$$v = (E - E')/(E - m_\mu), \tag{C.2}$$

where m_μ is the muon mass, and E' the muon energy after the interaction. For the root mean squared distributions $\langle\theta^2\rangle^{1/2}$ mentioned afterwards, the polar angle can be sampled from an exponential distribution as

$$\theta = \sqrt{\lambda \cdot \exp(-\lambda x)} \tag{C.3}$$

with $\lambda = \langle\theta^2\rangle$.

The parametrizations from GEANT4 have been reimplemented in PROPOSAL, based on their description given in [19].

C.1. Bremsstrahlung

C.1.1. Deflection parametrization of GEANT4, Tsai

In GEANT4 [19], angular distributions in $\theta_{\mu'}$ for the outgoing muon μ' and θ_γ for the photon γ can be sampled via

$$\theta_\gamma = \frac{m_\mu}{E}\, r, \qquad \theta_{\mu'} = \frac{E_{\text{loss}}}{E'}\, \theta_\gamma\,. \tag{C.4}$$

The variable r is defined as

$$r = \sqrt{\frac{a}{1-a}} \quad \text{with} \quad a = \xi\, \frac{r_{\max}^2}{1 + r_{\max}^2}\,. \tag{C.5}$$

Here, ξ is a random number uniformly distributed between 0 and 1 and the maximum $r_{\max}$ can be found as

$$r_{\max} = \min\left(1, \frac{E'}{E_{\text{loss}}}\right) \cdot \frac{E}{m_\mu}\, \theta^*\,. \tag{C.6}$$

In this parametrization, the small-angle, ultrarelativistic approximation $E \gg m_\mu$ is assumed which provides an accuracy of ∼20% at angles of $\theta \leq \theta^* \approx 1$. The LPM effect leads to a suppression at energies $E \leq 10^{20}$ eV which serves as an upper limit. Due to rising of Ter-Mikaelyan at lower energy transfers, a lower limit is set to $v_{\text{loss}} \geq 10^{-6}$, but bremsstrahlung is subdominant at such low v_{loss} [23].

C.1.2. Deflection parametrization from Van Ginneken

Based on the Mo-Tsai differential cross section $\mathrm{d}\sigma / \mathrm{d}p\,\mathrm{d}\Omega$ with momentum p and solid angle Ω of the particle after photon emission, a fit of the muon deflection angle is derived by Van Ginneken [17]. The RMS angle of an incoming muon of energy E scattering at a nucleus with atomic number Z is found as

$$\langle\theta^2\rangle^{1/2} = \begin{cases} \max\left[\min(k_1 v^{1/2}, k_2), k_3 v\right] & , v \leq 0.5 \\ k_4 v^{1+n}(1-v)^{-n} & , \langle\theta^2\rangle^{1/2} < 0.2, v > 0.5 \\ k_5 (1-v)^{-1/2} & , \langle\theta^2\rangle^{1/2} \geq 0.2, v > 0.5\,. \end{cases} \tag{C.7}$$

The additional parameters for muons are defined as

$$k_1 = 0.092 E^{-1/3}, \qquad k_2 = 0.052 E^{-1} Z^{-1/4},$$
$$k_3 = 0.22 E^{-0.92}, \qquad k_4 = 0.26 E^{-0.91},$$
$$k_5 = k_4 v_{\text{g}}^{1+n}(1 - v_{\text{g}})^{0.5-n}, \qquad n = 0.81 E^{0.5}/(E^{0.5} + 1.8),$$

where v_{g} follows with continuity at $\langle\theta^2\rangle^{1/2} = 0.2\,, v > 0.5$.

C.2. Electron-positron pair production

C.2.1. Deflection parametrization from Van Ginneken

A differential cross section for pair production is derived by Kelner [55]. A fit for the RMS muon deflection is performed by Van Ginneken as

$$\langle\theta^2\rangle^{1/2} = (2.3 + \ln(E))\, \frac{1}{E v^2}\, (1-v)^n \left(v - \frac{2m_e}{E}\right)^2 \times \min\left[\, f(v, E, a, b, c, d), e\,\right], \tag{C.8}$$

with

$$f = a\, v^{1/4}(1 + b\, E) + \frac{c\, v}{v + d}. \tag{C.9}$$

For muons, the parameters in the parametrization are defined as

$$n = -1, \qquad a = 8.9 \times 10^{-4}, \qquad b = 1.5 \times 10^{-5},$$
$$c = 0.0032, \qquad d = 1.0, \qquad e = 0.1.$$

A dependence on the charge number Z is neglected. A minimum energy transfer $E_{\text{loss,min}} = E - E'_{\max}$ follows as

$$v_{\min} = \frac{2m_e}{E} \tag{C.10}$$

$$\Leftrightarrow \qquad E_{\text{loss,min}} = 2m_e \left(1 - \frac{m}{E}\right) < 2m_e\,. \tag{C.11}$$

In practical use the limit is set to $v_{\text{min,p}} \approx 4m_e/E$ [56] due to the relativistic approximations in the cross sections used.

C.3. Ionization

C.3.1. Deflection parametrization by kinematics

A calculation via four-momentum conservation is performed to determine the resulting deflection of the incoming muon. The interaction is expressed by

$$P_\mu + P_e = P_{\mu'} + P_{e'}\,, \tag{C.12}$$

where P_i and $P_{i'}$ describe the incoming and outgoing four-momenta of the interacting muon and electron. To calculate the resulting deflection θ of the incoming muon, the following assumptions are used:

- $E_{e'} = E_\mu - E_{\mu'} + E_e$: The resulting electron energy depends on the electron energy before the interaction in addition to the total energy loss of the muon due to energy conservation.
- $\vec{p}_e^{\,2} \approx 0 \Rightarrow E_e \approx m_e$: The atomic electron rests before the interaction.

By squaring and transforming Equation (C.12) using the previously mentioned assumptions, the muon deflection can be found as

$$\theta = \arccos\left(\frac{(E_\mu + m_e)E_{\mu'} - E_\mu m_e - m_\mu^2}{|\vec{p}_\mu| \cdot |\vec{p}_{\mu'}|}\right). \tag{C.13}$$

C.4. Photonuclear interaction

C.4.1. Deflection parametrization of GEANT4

To sample muon deflection angles due to photonuclear interaction, in GEANT4 [19] the differential cross section is written as

$$\frac{\mathrm{d}\sigma}{\mathrm{d}t} \sim \frac{\left(1 - \frac{t}{t_{\max}}\right)}{t\left(1 + \frac{t}{E_{\text{loss}}^2}\right)\left(1 + \frac{t}{m_0^2}\right)} \left[(1 - v_{\text{loss}})\left(1 - \frac{t_{\min}}{t}\right) + \frac{v_{\text{loss}}^2}{2}\right], \tag{C.14}$$

with the assumption of four-momentum transfers $Q^2 \leq 3$ GeV^2 [57,58]. Here, the definition $t = Q^2 = 2(EE' - PP'\cos\theta - m_\mu^2)$ is used with the parameters

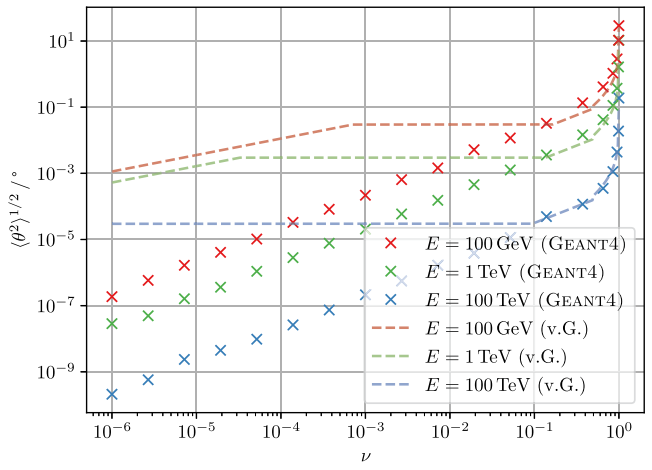

(a) Root mean squared deflections due to bremsstrahlung parametrized by GEANT4 are lower than those determined by Van Ginneken for very small energy transfers. In GEANT4, an approximation of bremsstrahlung in the Coulomb filed of an unshielded nucleus is used, what leads to the non-appearance of the plateau. At high ν, the agreement is better. The atomic number is set to $Z = 1$.

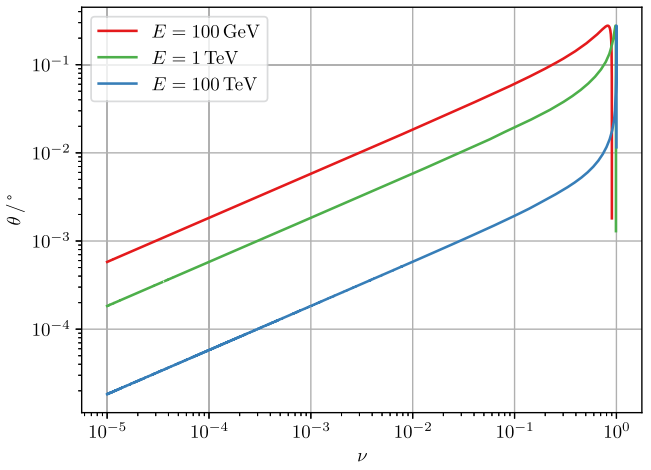

(b) Calculation of deflection due to ionization is shown. For very high energy transfers, the deflection approaches zero due to a vanishing transverse momentum. All distributions peak with $\theta = 0.277°$. Maximum energy transfers result to minimum final energies $E'(E = 100\,\mathrm{GeV}) > 9.85\,\mathrm{GeV}$, $E'(E = 1\,\mathrm{TeV}) > 10.81\,\mathrm{GeV}$ and $E'(E = 100\,\mathrm{TeV}) > 10.92\,\mathrm{GeV}$.

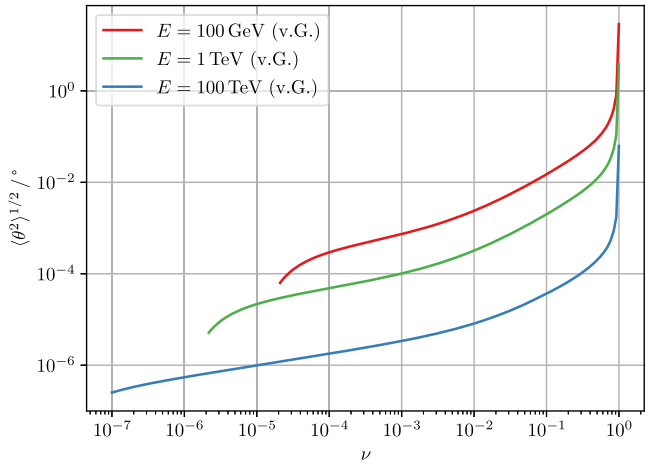

(c) Root mean squared deflections for electron pair production, parametrized by Van Ginneken, are shown. For very small relative energy transfers ν, the deflection increases sharply.

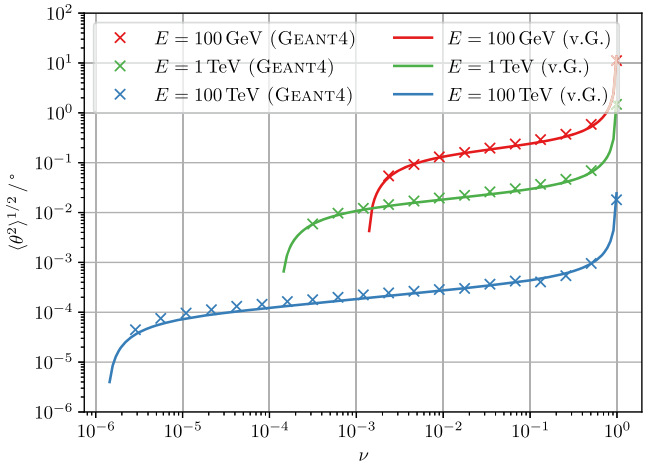

(d) Root mean squared deflections due to photonuclear interactions are parametrized by Van Ginneken and GEANT4 with minimum energy transfers $\nu_{\mathrm{min,\,GEANT4}} = 200\,\mathrm{MeV}$ and $\nu_{\mathrm{min,\,v.G.}} = 136\,\mathrm{MeV}$.

Fig. C.15. All parametrizations to describe deflections by stochastic interactions implemented in PROPOSAL are presented for three different energies in dependence of the relative energy transfer $\nu = (E - E')/(E - m)$ with the initial particle energy E, the remaining energy E' after the interaction and the muon mass m. In each sampling, 100 000 angles are drawn. For bremsstrahlung and photonuclear interaction, there are two parametrizations available each by Van Ginneken (v.G.) [17] and GEANT4 [19]. The lower the energy, the larger the deflection. Bigger energy transfers result in larger deflections.

$$t_{\min} = \frac{(m_\mu\, \nu_{\mathrm{loss}})^2}{1 - \nu_{\mathrm{loss}}}, \qquad \nu_{\mathrm{loss}} = \frac{E_{\mathrm{loss}}}{E},$$

$$t_{\max} = 2M\,E_{\mathrm{loss}}, \qquad E_{\mathrm{loss}} = E - E',$$

with the nucleon (here proton) mass M, and $m_0^2 \equiv \Lambda^2 \approx 0.4\ \mathrm{GeV}^2$, which is a phenomenological parameter determining the behavior of the inelastic form factor. Weak interaction factors are neglected on t. Equation (C.14) can be written as

$$\sigma(t) \sim f(t)\, g(t), \tag{C.15}$$

with two substitutions

$$f(t) = \frac{1}{t\left(1 + \frac{t}{t_1}\right)},$$

$$g(t) = \frac{1 - \frac{t}{t_{\max}}}{1 + \frac{t}{t_2}} \cdot \frac{(1 - \nu_{\mathrm{loss}})\left(1 - \frac{t_{\min}}{t}\right) + \frac{\nu_{\mathrm{loss}}^2}{2}}{(1 - \nu_{\mathrm{loss}}) + \frac{\nu_{\mathrm{loss}}^2}{2}}, \tag{C.16}$$

and

$$t_1 = \min(E_{\mathrm{loss}}^2, m_0^2), \qquad t_2 = \max(E_{\mathrm{loss}}^2, m_0^2). \tag{C.17}$$

Solving Equations (C.16) analytically leads to

$$t_P = \frac{t_{\max} t_1}{(t_{\max} + t_1)\left[\frac{t_{\max}(t_{\min}+t_1)}{t_{\min}(t_{\max}+t_1)}\right]^{\xi} - t_{\max}}, \tag{C.18}$$

with a random number $\xi \in (0,1)$ and acceptance of probability $g(t)$. From this, the polar muon deflection angle θ can be derived as [19]

$$\theta = 2 \cdot \arcsin\left(\sqrt{\frac{t_P - t_{\min}}{4(EE' - m_\mu^2) - 2t_{\min}}}\right). \tag{C.19}$$

A minimum energy loss of 200 MeV and a maximum energy transfer of $E - M/2$ with M as the nucleon (proton) mass is recommended.

C.4.2. Deflection parametrization from Van Ginneken

Using a lepto-production scaling formula from [59], Van Ginneken has fit the RMS angle of the outgoing muon as

$$\langle\theta^2\rangle^{1/2} = \frac{0.39}{E(1-\nu)}(E^{1/2}\nu(1-\nu))^{0.17} \cdot \left(1 - \frac{0.135}{E\nu}\right). \tag{C.20}$$

A minimum energy transfer results to about 136 MeV since this is the mass of the pion, which is the lightest hadron that can be produced [17].

Appendix D. Electron and positron interactions

D.1. Ionization

Ionization describes the energy loss due to collisions with atomic electrons. For energy transfers high compared to the binding energies of atomic electrons, the ionization process can be considered a scattering process on free electrons and, therefore, described by Møller and Bhabha scattering. In this case, the differential cross section is given for $T \gg I$, with T the kinetic energy of the secondary electron and I the ionization energy of the target atom, as

$$\frac{d\sigma}{d\epsilon} = \frac{2\pi r_e^2 Z}{\beta^2(\gamma-1)}\left[\frac{(\gamma-1)^2}{\gamma^2} + \frac{1}{\epsilon}\left(\frac{1}{\epsilon} - \frac{2\gamma-1}{\gamma^2}\right) + \frac{1}{1-\epsilon}\left(\frac{1}{1-\epsilon} - \frac{2\gamma-1}{\gamma^2}\right)\right] \tag{D.1}$$

for Møller scattering $e^-e^- \to e^-e^-$, and

$$\frac{d\sigma}{d\epsilon} = \frac{2\pi r_e^2 Z}{\gamma-1}\left[\frac{1}{\beta^2\epsilon^2} - \frac{B_1}{\epsilon} + B_2 - B_3\epsilon + B_4\epsilon^2\right] \tag{D.2}$$

for Bhabha scattering $e^+e^- \to e^+e^-$. Here, $\epsilon = T/(E - mc^2)$ with E the initial electron/positron energy. The kinematic limits of ϵ are given as

$$\epsilon_0 = \frac{T_{\text{cut}}}{E - mc^2} \le \epsilon \le \frac{1}{2}, \text{ for } e^-e^-, \tag{D.3}$$

$$\epsilon_0 = \frac{T_{\text{cut}}}{E - mc^2} \le \epsilon \le 1, \text{ for } e^+e^-. \tag{D.4}$$

Here T_{cut} denotes a threshold energy. The quantities B_i are given by

$$B_1 = 2 - y^2, \qquad \gamma = E/mc^2, \tag{D.5}$$

$$B_2 = (1-2y)(3+y^2), \qquad \beta^2 = 1 - 1/\gamma^2, \tag{D.6}$$

$$B_3 = (1-2y)^2 + (1-2y)^3, \qquad y = \frac{1}{\gamma+1}, \tag{D.7}$$

$$B_4 = (1-2y)^3. \tag{D.8}$$

The electron binding energies need to be considered for small energy transfers, which are relevant for calculating continuous energy losses. This continuous energy loss is described by the parametrization by Berger and Seltzer [60], which is used in PROPOSAL to describe continuous ionization losses for electrons and positrons. It is given by

$$-\left(\frac{\mathrm{d}E}{\mathrm{d}X}\right) = \frac{2\pi r_e^2 m_e}{\beta^2}\left[\ln\left(\frac{2m_e(\tau+2)}{I}\right) + F^{\pm}(\tau,\Delta) - \delta\right], \tag{D.9}$$

with the mean ionization energy I, and

$$\tau = \gamma - 1, \qquad \Delta = \min\left(\frac{v_{\max}E}{m_e}, \frac{v_{\text{cut}}E}{m_e}\right). \tag{D.10}$$

For the density correction δ, the parametrization by Sternheimer [61] is used. The term $F^{\pm}(\tau,\Delta)$ is given by

$$F^-(\tau,\Delta) = -1 - \beta^2 + \ln((\tau-\Delta)\Delta) + \frac{\tau}{\tau-\Delta} + \frac{1}{\gamma^2}\left[\frac{\Delta^2}{2} + (2\tau+1)\ln\left(1 - \frac{\Delta}{\tau}\right)\right] \tag{D.11}$$

for electrons, and

$$F^+(\tau,\Delta) = \ln(\tau\Delta) - \frac{\beta^2}{\tau}\left[\tau + 2\Delta - \frac{3\Delta^2 y}{2} - (\Delta - \frac{\Delta^2}{3})y^2 - (\frac{\Delta^2}{2} - \frac{\tau\Delta^3}{3} + \frac{\Delta^4}{4})y^3\right] \tag{D.12}$$

for positrons. Fig. D.16 shows the average ionization energy loss of electrons and positrons.

D.2. Bremsstrahlung

For energies above 50 MeV, the ultra-relativistic differential cross section, comparable to the Complete Screening parametrization, which has already been implemented in PROPOSAL, is given by [34,62]

$$\frac{d\sigma}{dv} = \frac{Z(Z+\xi(Z))r_e^2\alpha}{v}\left[(2 - 2v + v^2)\left(\Phi_1(x) - \frac{4}{3}\ln(Z) - 4f_c(Z)\right) - \frac{2}{3}(1-v)\left(\Phi_2(x) - \frac{4}{3}\ln(Z) - 4f_c(Z)\right)\right], \tag{D.13}$$

with the relative energy loss v, and

$$x = 136Z^{-1/3}\frac{2\delta}{m_e}, \qquad \delta = \frac{m_e^2 v}{2E(1-v)}. \tag{D.14}$$

The functions $\Phi_1(x)$, $\Phi_2(x)$ describe the screening effects and are given by

$$\Phi_1(x) = \begin{cases} 20.867 - 3.242x + 0.625x^2 & \text{if } x \le 1, \\ 21.12 - 4.184\ln(x + 0.952) & \text{if } x > 1, \end{cases} \tag{D.15}$$

$$\Phi_2(x) = \begin{cases} 20.029 - 1.930x - 0.086x^2 & \text{if } x \le 1, \\ 21.12 - 4.184\ln(x + 0.952) & \text{if } x > 1, \end{cases} \tag{D.16}$$

which is an analytical approximation of the Thomas-Fermi form factors [63]. Furthermore, $f_c(Z)$ describes the Coulomb correction and is approximated in an analytical form by [64]

$$f_c(Z) \approx a^2\left[\frac{1}{1+a^2} + 0.20206 - 0.0369a^2 + 0.0083a^4 - 0.002a^6\right] \tag{D.17}$$

with $a = \alpha Z$. The parameter

$$\xi(Z) = \frac{L'_{\text{rad}}(Z)}{L_{\text{rad}}(Z) - f_c(Z)} \tag{D.18}$$

with the radiation logarithms [35]

$$L'_{\text{rad}} = \begin{cases} \ln(1194Z^{-2/3}) & \text{if } Z > 4, \\ 5.924 & \text{if } Z = 4, \\ 5.805 & \text{if } Z = 3, \\ 5.621 & \text{if } Z = 2, \\ 6.144 & \text{if } Z = 1, \end{cases} \tag{D.19}$$

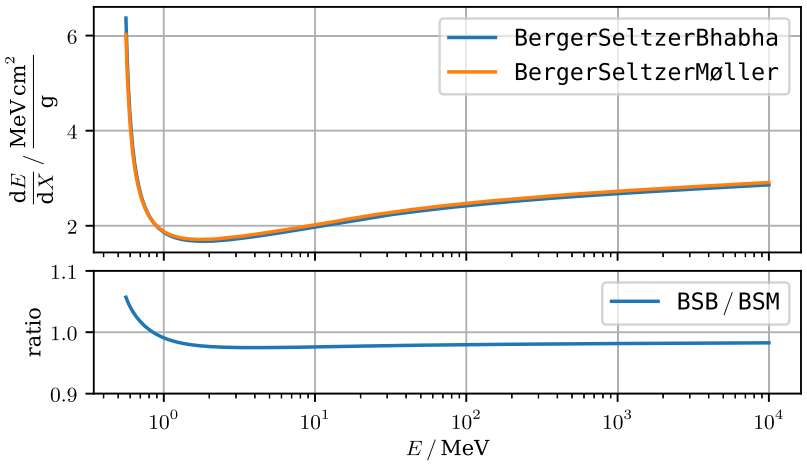

Fig. D.16. Continuous energy losses of electrons (Møller) and positrons (Bhabha) in air.

$$L_{\text{rad}} = \begin{cases} \ln(184.15 Z^{-1/3}) & \text{if } Z > 4, \\ 4.710 & \text{if } Z = 4, \\ 4.740 & \text{if } Z = 3, \\ 4.790 & \text{if } Z = 2, \\ 5.310 & \text{if } Z = 1, \end{cases} \tag{D.20}$$

accounts for atomic electron effects.

For energies below 50 MeV, the differential bremsstrahlung cross section is given by

$$\frac{d\sigma}{dv} = \frac{A'(E,Z)Z(Z+\xi(Z))r_e^2\alpha}{v}\left[(2-2v+v^2)\left(\Phi_1(x)-\frac{4}{3}\ln(Z)\right) - \frac{2}{3}(1-v)\left(\Phi_2(x)-\frac{4}{3}\ln(Z)\right)\right] \tag{D.21}$$

where a density correction factor $A'(E,Z)$ has been introduced [65]. This factor $A'(E,Z)$ rescales the differential cross section to agree with the empirical average energy losses per distance from [66]. It should be noted that this factor is only a normalization factor and is, therefore, not affecting the shape of the energy loss distribution.

D.3. Electron-positron pair production

The cross section for the process of triplet pair production $e^\pm + Z \to e^\pm + e^+ + e^- + Z$ was adapted from the cross section for muon-induced muon pair production $\mu^\pm + Z \to \mu^\pm + \mu^+ + \mu^- + Z$ of [13], removing the nuclear form factor correction, which for electrons is negligible in contrast to muons. The cross section is parametrized by

$$\frac{d\sigma}{dv\,d\rho} = \frac{2}{3\pi}(Z\alpha r_e)^2\frac{1-v}{v}\Phi\ln X, \tag{D.22}$$

where

$$\Phi = [(2+\rho^2)(1+\beta)+\xi(3+\rho^2)]\ln\left(1+\frac{1}{\xi}\right) + \left[(1+\rho^2)\left(1+\frac{3}{2}\beta\right)-\frac{1+2\beta}{\xi}(1-\rho^2)\right]\ln(1+\xi) - 1 - 3\rho^2 + \beta(1-2\rho^2), \tag{D.23}$$

$$X = 1 + U(E,v,\rho) - U(E,v,\rho_{\max}), \tag{D.24}$$

$$U(E,v,\rho) = \frac{BZ^{-1/3}}{1+\frac{2\sqrt{e}mBZ^{-1/3}(1+\xi)(1+Y)}{Ev(1-\rho^2)}} \tag{D.25}$$

with

$$\beta = \frac{v^2}{2(1-v)}, \qquad \xi = \frac{v^2(1-\rho^2)}{4(1-v)},$$
$$\rho_{\max} = 1 - \frac{2m}{Ev}, \qquad Y = 12\sqrt{m/E}.$$

D.4. Annihilation

The total cross section for annihilation of a positron with Lorentz factor γ on an atomic electron at rest is given by [67,19]

$$\sigma(\gamma) = \frac{\pi r_e^2}{\gamma+1}\left[\frac{\gamma^2+4\gamma+1}{\gamma^2-1}\ln(\gamma+\sqrt{\gamma^2-1}) - \frac{\gamma+3}{\sqrt{\gamma^2-1}}\right]. \tag{D.26}$$

The differential cross section for annihilation into two photons is given by

$$\frac{d\sigma}{d\epsilon} = \frac{\pi r_e^2}{\gamma-1}\frac{1}{\epsilon}\left[1+\frac{2\gamma}{(\gamma+1)^2}-\epsilon-\frac{1}{(\gamma+1)^2}\frac{1}{\epsilon}\right], \tag{D.27}$$

where ϵ is the dimensionless photon energy $\epsilon = E_\gamma/mc^2$, which has the limits

$$\epsilon_{\text{min, max}} = \frac{1}{2}\left[1 \pm \sqrt{\frac{\gamma-1}{\gamma+1}}\right]. \tag{D.28}$$

The final state kinematics can be determined from energy-momentum conservation. The scattering angle θ between the incident positron and the photon with energy ϵ is given by

$$\cos\theta = \frac{\epsilon(\gamma+1)-1}{\epsilon\sqrt{\gamma^2-1}}. \tag{D.29}$$

Appendix E. Photon interactions

E.1. Compton scattering

The differential Klein-Nishina cross section for scattering of a photon with energy ω_0 to a final state with photon energy

$$\omega_1 = \frac{\omega_0}{1+(\omega_0/m)(1-\cos\theta)}, \tag{E.1}$$

where θ is the scattering angle, is given by [68]

$$\frac{d\sigma}{d\Omega} = \frac{Zr_e^2}{2}\left(\frac{\omega_0}{\omega_1}\right)^2\left[4\left(\frac{m}{2\omega_1}-\frac{m}{2\omega_0}\right)^2 - 4\left(\frac{m}{2\omega_1}-\frac{m}{2\omega_0}\right) - \left(\frac{\omega_1}{\omega_0}+\frac{\omega_0}{\omega_1}\right)\right]. \tag{E.2}$$

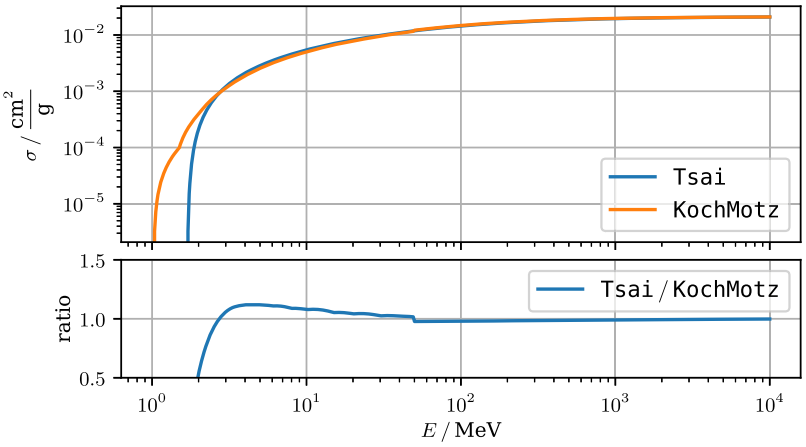

Fig. E.17. Total cross section of electron-positron pair production in air for the parametrizations according to (E.5) (`Tsai`) and (E.8) (`KochMotz`).

With the Compton relation (E.1), the cross section differential in ω_1 is given by

$$\frac{d\sigma}{d\omega_1} = Z\pi r_e^2 \frac{\omega_0^2 m}{\omega_1^4}\left[4\left(\frac{m}{2\omega_1}-\frac{m}{2\omega_0}\right)^2 - 4\left(\frac{m}{2\omega_1}-\frac{m}{2\omega_0}\right) - \left(\frac{\omega_1}{\omega_0}+\frac{\omega_0}{\omega_1}\right)\right]. \tag{E.3}$$

The total cross section can be calculated analytically as

$$\sigma(\epsilon) = Z\frac{\pi r_e^2}{\epsilon^2}\left(4+\frac{2\epsilon^2(1+\epsilon)}{(1+2\epsilon)^2}+\frac{\epsilon^2-2\epsilon-2}{\epsilon}\ln(1+2\epsilon)\right), \tag{E.4}$$

where $\epsilon = E_\gamma/m_e c^2$ is the photon energy in the electron rest frame in units of the electron rest mass.

E.2. Electron-positron pair production

In PROPOSAL, the process of electron-positron pair production can be described by two different parametrizations presented in this section. Fig. E.17 compares the two parametrizations. Furthermore, the LPM suppression for this process has been implemented.

E.2.1. Tsai parametrization

The process of electron-positron pair production is described by quantum electrodynamics, and a differential cross section exact to order α^3 is provided by [35]. However, evaluating this expression is too complicated for a direct implementation. Based on [35], an approximated expression is given by

$$\frac{d\sigma}{dx} = \frac{\alpha r_e^2 x E_\gamma}{p}\left\{\left(\frac{4}{3}x^2-\frac{4}{3}x+1\right)\times\left[Z^2\left(\varphi_1-\frac{4}{3}\ln(Z)-4f(z)\right)+Z\left(\psi_1-\frac{8}{3}\ln(Z)\right)\right] - \frac{2}{3}x(1-x)\left[Z^2\left(\varphi_1-\varphi_2\right)+Z\left(\psi_1-\psi_2\right)\right]\right\} \tag{E.5}$$

with $x = E_-/E_\gamma$, where E_γ is the energy of the initial photon, E_- the energy of the produced electron, and p its absolute momentum. The function $f(z)$ describes the Coulomb correction and is defined as [35]

$$f(z) = 1.202z - 1.0369z^2 + 1.008\frac{z^3}{1+z}, \qquad z = \left(\frac{Z}{137}\right)^2. \tag{E.6}$$

While the approximate differential cross section ignores effects from nuclear form factors, which are only important for large production angles, the effects from the atomic form factors are described by the functions φ_1, φ_2 (elastic scattering part) and ψ_1, ψ_2 (inelastic scattering part). The description used for the atomic form factors varies with Z, and the resulting expressions for φ and ψ are given in [35].

Since the photon must provide the rest mass of both the electron and the positron, the kinematic limits of the process are given by

$$E \geq 2m_e, \qquad x_{\min} = \frac{m_e}{E_\gamma}, \qquad x_{\max} = 1-\frac{m_e}{E_\gamma}. \tag{E.7}$$

E.2.2. Koch and Motz parametrization

The cross section of electron-positron pair production is given analogously to the bremsstrahlung cross section in Appendix D.2. Above 50 MeV, the cross section is given by [62]

$$\frac{d\sigma(Z,E,v)}{dx} = Z(Z+\xi(Z))r_0^2\alpha\left\{(2x^2-2x+1)\left[\Phi_1(\delta)-\frac{4}{3}\ln Z-4f_c(Z)\right] + \frac{2}{3}x(1-x)\left[\Phi_2(\delta)-\frac{4}{3}\ln Z-4f_c(Z)\right]\right\}, \tag{E.8}$$

where

$$\delta = \frac{136 m_e Z^{-1/3}}{E_\gamma x(1-x)}. \tag{E.9}$$

The structure functions $\Phi_{1,2}$ are identical to the bremsstrahlung case. Again, for energies below 50 MeV, an empirical correction factor is used, with cross section data taken from [69].

E.2.3. LPM effect

The suppression of the electron-positron pair production cross section due to the LPM effect has been implemented based on the parametrization given in [70] and is defined as

$$\frac{\mathrm{d}\sigma_{\mathrm{LPM}}}{\mathrm{d}x} = \frac{\mathrm{d}\sigma}{\mathrm{d}x}\cdot\frac{\xi(s)/3\left(G(s)+2\left(x^2+(1-x)^2\right)\phi(s)\right)}{1-4/3x(1-x)}. \tag{E.10}$$

For $\xi(s)$, $G(s)$, and $\phi(s)$, the definitions by [22,71] are used, which are given by

$$\xi(s) \approx \xi(s') = \begin{cases} 2 & \text{if } s' < s_1, \\ 1+h-\frac{0.08(1-h)(1-(1-h)^2)}{\ln(s_1)} & \text{if } s_1 \leq s' < 1, \\ 1 & \text{if } s' \geq 1, \end{cases} \tag{E.11}$$

$$G(s) = \begin{cases} 3\psi(s)-2\phi(s) & \text{if } s < 0.710\,390, \\ 36s^2/\left(36s^2+1\right) & \text{if } 0.710\,390 \leq s < 0.904\,912, \\ 1-0.022s^{-4} & \text{if } s \geq 0.904\,912, \end{cases} \tag{E.12}$$

$$\psi(s) = 1-\exp\left\{-4s-\frac{8s^2}{1+3.936s+4.97s^2-0.05s^3+7.5s^4}\right\}, \tag{E.13}$$

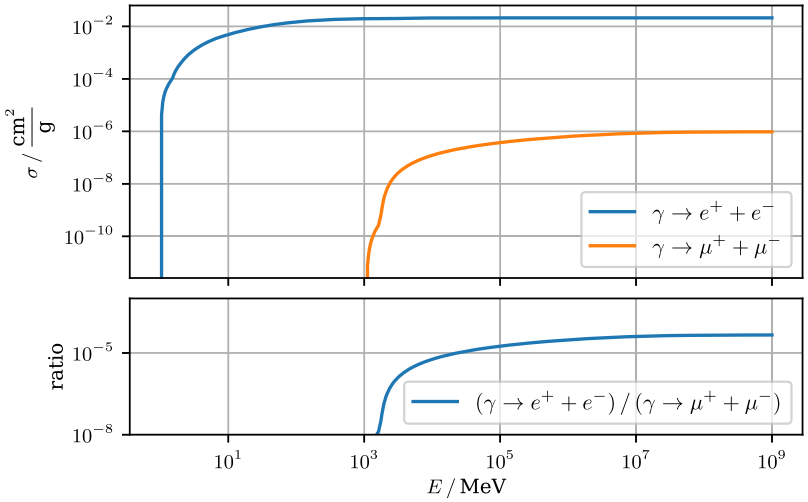

Fig. E.18. Total cross section of muon pair production in air, compared to the total cross section of electron-positron pair production according to (E.8).

$$\phi(s) = \begin{cases} 1 - \exp\left\{-6s\,(1+(3-\pi)s) + \frac{s^3}{0.623+0.796s+0.658s^2}\right\} \\ \quad \text{if } s < 1.549\,54, \\ 1 - 0.012 s^{-4} \\ \quad \text{if } s \geq 1.549\,54, \end{cases} \tag{E.14}$$

with

$$s = \frac{s'}{\sqrt{\xi(s')}}, \qquad s' = \frac{1}{8}\sqrt{\frac{E_{\mathrm{LPM}}}{Ex(1-x)}}, \qquad s_1 = \frac{\sqrt{2}Z^{2/3}}{B^2}, \tag{E.15}$$

$$E_{\mathrm{LPM}} = \frac{2\alpha(m_e c^2)^2 X_0}{\pi\hbar c}, \qquad h = \frac{\ln(s')}{\ln(s_1)}, \qquad D_n = 1.54 A^{0.27}. \tag{E.16}$$

Here, X_0 is the radiation length, and B is the radiation logarithm constant. The effect of the LPM effect on pair production can be seen in Fig. 7b.

E.3. $\mu^+\mu^-$ pair production

Muon pair production describes the conversion of a photon into a muon-antimuon pair in the field of an atomic nucleus. While the process is suppressed by a factor of approximately $\left(m_e/m_\mu\right)^2$ compared to the cross section of electron-positron pair production, it provides a significant contribution to the number of muons in electromagnetic air showers.

Using crossing symmetry, the differential cross section for muon pair production is obtained from the differential bremsstrahlung cross section of muons [72] and is given by

$$\frac{\mathrm{d}\sigma}{\mathrm{d}x} = 4Z^2\alpha\left(r_e\frac{m_e}{m_\mu}\right)^2 \Phi(\delta)\left[1 - \frac{4}{3}(x - x^2)\right], \tag{E.17}$$

with the definitions

$$\Phi(\delta) = \underbrace{\ln\left(\frac{BZ^{-1/3}m_\mu/m_e}{1 + BZ^{-1/3}\sqrt{e}\delta/m_e}\right)}_{\Phi_0} - \underbrace{\ln\left(\frac{D_n}{1+\delta(D_n\sqrt{e}-2)/m_\mu}\right)}_{\Delta_{\mathrm{n}}}, \tag{E.18}$$

where B is the material-dependent logarithm constant [73] and

$$x = \frac{E_{\mu^-}}{E}, \qquad \delta = \frac{m_\mu^2}{2Ex(1-x)}, \qquad D_n = 1.54A^{0.27}. \tag{E.19}$$

The contribution of atomic electrons is taken into account with

$$\Phi(\delta) \to \Phi(\delta) + \frac{1}{Z}\left[\ln\left(\frac{m_\mu/\delta}{\delta m_\mu/m_e^2 + \sqrt{e}}\right) - \ln\left(1 + \frac{1}{\delta\sqrt{e}B'Z^{-2/3}/m_e}\right)\right], \tag{E.20}$$

where B' is the inelastic radiation logarithm [73]. The effect of the inelastic nuclear form factor is taken into account with

$$\Delta_{\mathrm{n}} \to \left(1 - \frac{1}{Z}\right)\Delta_{\mathrm{n}} \tag{E.21}$$

for $Z > 1$. The kinematic limits in x are defined as

$$\frac{1}{2}\left(1 - \sqrt{1 - 2\sqrt{e}m_\mu/E}\right) \leq x \leq \frac{1}{2}\left(1 + \sqrt{1 - 2\sqrt{e}m_\mu/E}\right). \tag{E.22}$$

Fig. E.18 shows the total cross section for muon pair production, compared to electron-positron pair production.

E.4. Photoelectric interaction

Photoelectric interaction defines the absorption of a photon by an atom with the ejection of a formerly bound electron. In general, the cross section depends on the atomic structure of the target atom; however, if the energy of the photon is not near the energy of an absorption edge (of the order of a few keV to a few tens of keV), the cross section can be written in the Born approximation as ([74,75], cited after [67])

$$\sigma_{\mathrm{ph.el.}} = \sigma_{\mathrm{T}}\frac{3}{2}Z^5\alpha^4\left(\frac{m_e}{\omega}\right)^5(\gamma^2-1)^{3/2} \times \left[\frac{4}{3} + \frac{\gamma(\gamma-2)}{\gamma+1}\left(1 - \frac{1}{2\gamma\sqrt{\gamma^2-1}}\ln\frac{\gamma+\sqrt{\gamma^2-1}}{\gamma-\sqrt{\gamma^2-1}}\right)\right], \tag{E.23}$$

where ω is the incoming photon energy,

$$\gamma = 1 + \frac{\omega - I}{m_e} \tag{E.24}$$

is the Lorentz factor of the ejected electron, and $\sigma_{\mathrm{T}} = (8\pi/3)r_e^2$ is the Thomson cross section. $I = Z^2\alpha^2 m_e/2$ denotes the ionization energy of the K-shell electron.

The result above uses the Born approximation, i.e., plane wave functions. Therefore it applies mainly to light elements. The argument of the logarithm can be rewritten as

$$\frac{\gamma+\sqrt{\gamma^2-1}}{\gamma-\sqrt{\gamma^2-1}} = \frac{(\gamma+\sqrt{\gamma^2-1})^2}{\gamma^2-(\sqrt{\gamma^2-1})^2} = (\gamma+\sqrt{\gamma^2-1})^2 \tag{E.25}$$

to avoid numerical problems at $\gamma \gg 1$.

In [75], a correction factor for the nonrelativistic region is calculated

$$F = |\Gamma(2+n)|^2 e^{i\pi n - 4in \arctan(1/in)} \tag{E.26}$$

with $n = \alpha Z/i\beta$. This can be rewritten as

$$F = \left[1 + \left(\frac{Z\alpha}{\beta}\right)^2\right] \frac{\alpha Z\pi/\beta}{\sinh(\alpha Z\pi/\beta)} \exp\left[\frac{Z\alpha}{\beta}\left(\pi - 4\arctan\frac{\beta}{\alpha Z}\right)\right]. \tag{E.27}$$

Including this prefactor improves the agreement in comparison to more detailed calculations.

The cross section in (E.23) describes the dominant absorption on the K-shell electron. An empirical formula from [76] for the ratio of the K-shell and the total photoelectric cross section is given by

$$\frac{\tau_{pe}}{\tau_K} = 1 + 0.014\,81 \ln^2 Z - 0.000\,788 \ln^3 Z. \tag{E.28}$$

This parametrization is used as a correction factor to (E.23) to obtain a better description of the total photoelectric cross section.

Appendix F. Secondary parametrizations

F.1. Bremsstrahlung by electrons and positrons

The implemented `KochMotzSampling` method to sample the production angle of bremsstrahlung photons is based on the double differential cross section by Koch and Motz [34]. The underlying rejection sampling method is adapted from [28] and described in more detail in [77]. Firstly, a candidate scattering angle $\hat{\theta}$ is sampled via

$$\hat{\theta} = \frac{m_e}{E}\sqrt{\frac{\xi_1}{1 - \xi_1 + \left(\frac{m_e}{\pi E}\right)^2}}, \tag{F.1}$$

with a random number $\xi_1 \in [0, 1)$. Next, the normalization of the rejection function is calculated from

$$N_r = 1 \,/\, \max\left[g(0), g(1), g\left(\frac{\pi^2 E^2}{m_e^2}\right)\right] \tag{F.2}$$

with the definitions

$$g(x) = 3\left(1 + r^2\right) - 2r - (4 + \ln(m(x)))\left(\left(1 + r^2\right) - \frac{4xr}{(1+x)^2}\right), \tag{F.3}$$

$$m(x) = \left(\frac{m_e(1-r)}{2rE}\right)^2 + \left(\frac{Z^{1/3}}{111(1+x)}\right)^2, \tag{F.4}$$

and $r = 1 - v$. The scattering angle $\hat{\theta}$ is accepted when the condition

$$\xi_2 \leq N_r \cdot g\left(\frac{E^2 \cdot \hat{\theta}^2}{m_e^2}\right) \tag{F.5}$$

is fulfilled, using an additional random number ξ_2. If this is not the case, the process is repeated from equation (F.1), using a new set of random numbers (ξ_1, ξ_2).

F.2. Electron-positron pair production

An approximative double differential cross section describing the angular distribution of electron-positron pair production based on [35] is given by

$$\frac{d^2\sigma}{d\theta dp} = \frac{2\alpha^3 E_-^2}{\pi E_\gamma m_e^4}\sin(\theta)\left[\left(\frac{2x(1-x)}{(1+l)^2} - \frac{12lx(1-x)}{(1+l)^4}\right)G_2(\infty) + \left(\frac{2x^2 - 2x + 1}{(1+l)^2} + \frac{4lx(1-x)}{(1+l)^4}\right)\left(X - 2Z^2 f(z)\right)\right], \tag{F.6}$$

with the angle θ between the initial photon of energy E_γ and produced electron with energy E_-, and

$$x = \frac{E_-}{E_\gamma}, \qquad l = \frac{E_-^2\theta^2}{m_e^2}, \qquad G_2(\infty) = Z^2 + Z.$$

The function X, describing the influence of atomic form factors, varies with Z and is defined in [35]. The angle θ can be sampled from this differential cross section by solving the integral equation

$$\left(\frac{d\sigma}{dp}\right)^{-1}\int_0^\theta \frac{d^2\sigma}{d\theta dp}\,d\theta = \xi, \tag{F.7}$$

with a random number $\xi \in [0, 1)$. This method is called `Tsai`.

An alternative approach is given based on the leading term of the differential cross section in [36], which is given by

$$\frac{d\sigma}{d\theta_\pm} \propto \frac{\sin(\theta_\pm)}{2p_\pm\left(E_\pm - p_\pm\cos(\theta_\pm)\right)^2}. \tag{F.8}$$

The deflection angle θ can be sampled with [62]

$$\cos(\theta_\pm) = \frac{E_\pm(2\xi - 1) + p_\pm}{p_\pm(2\xi - 1) + E_\pm}, \tag{F.9}$$

using a random number $\xi \in [0, 1)$. This method is called `Sauter`.

Appendix G. Default parametrizations

When the method `GetStdCrossSections()` (C++) or `make_std_crosssection()` (Python) is called, PROPOSAL returns a list of cross sections, using parametrizations that are reasonable for the given particle type. The specific parametrizations are listed in Tables G.4, G.5, G.6, and G.7.

Table G.4
Default energy loss parametrizations for electrons.

Interaction type	Parametrization name	Reference
Bremsstrahlung	`ElectronScreening`	Appendix D.2
e^-e^+ pair production	`ForElectronPositron`	Appendix D.3
Ionization	`BergerSeltzerMoller`	Appendix D.1
Photonuclear	`AbramowiczLevinLevyMaor97`	[78,79]

Table G.5
Default energy loss parametrizations for positrons.

Interaction type	Parametrization name	Reference
Bremsstrahlung	`ElectronScreening`	Appendix D.2
e^-e^+ pair production	`ForElectronPositron`	Appendix D.3
Ionization	`BergerSeltzerBhabha`	Appendix D.1
Photonuclear	`AbramowiczLevinLevyMaor97`	[78,79]
Annihilation	`Heitler`	Appendix D.4

Table G.6
Default energy loss parametrizations for photons.

Interaction type	Parametrization name	Reference
Pair production	`KochMotz`	Appendix E.2.2
Compton	`KleinNishina`	Appendix E.1
Photoproduction	`Rhode`	[80]
Photoeffect	`Sauter`	Appendix E.4

Table G.7
Default energy loss parametrizations for muons and taus.

Interaction type	Parametrization name	Reference
Bremsstrahlung	`KelnerKokoulinPetrukhin`	[72]
e^-e^+ pair production	`KelnerKokoulinPetrukhin`	[81,82]
Ionization	`BetheBlochRossi`	[83,84]
Photonuclear	`AbramowiczLevinLevyMaor97`	[78,79]

Table G.8
Default and optional stochastic deflection parametrizations for muons.

Interaction type	Parametrization name	Reference
Bremsstrahlung	`BremsTsaiApproximation`	Appendix C.1.1
(optional)	`BremsGinneken`	Appendix C.1.2
e^-e^+ pair production	`EpairGinneken`	Appendix C.2.1
Ionization	`IonizNaive`	Appendix C.3.1
Photonuclear	`PhotoBorogPetrukhin`	Appendix C.4.1
(optional)	`PhotoGinneken`	Appendix C.4.2

Furthermore, the parametrizations for the stochastic deflections are presented in Table G.8. Note that for stochastic deflections, currently, only parametrizations valid and tested for muons are provided.

References

[1] J.-H. Koehne, et al., PROPOSAL: a tool for propagation of charged leptons, Comput. Phys. Commun. 184 (2013) 2070–2090, https://doi.org/10.1016/j.cpc.2013.04.001.

[2] D.A. Chirkin, W. Rhode, Propagating leptons through matter with Muon Monte Carlo (MMC), arXiv:hep-ph/0407075, 2004.

[3] V. Kudryavtsev, Muon simulation codes MUSIC and MUSUN for underground physics, Comput. Phys. Commun. 180 (2009) 339–346, https://doi.org/10.1016/j.cpc.2008.10.013, arXiv:0810.4635.

[4] I.A. Sokalski, E.V. Bugaev, S.I. Klimushinm, MUM: flexible precise Monte Carlo algorithm for muon propagation through thick layers of matter, Phys. Rev. D 64 (2001) 074015, https://doi.org/10.1103/PhysRevD.64.074015, arXiv:hep-ph/0010322.

[5] V. Niess, The PUMAS library, Comput. Phys. Commun. 279 (2022) 108438, https://doi.org/10.1016/j.cpc.2022.108438, arXiv:2206.01457.

[6] R. Abbasi, et al., Improved characterization of the astrophysical Muon–neutrino flux with 9.5 years of IceCube data, Astrophys. J. 928 (2022) 50, https://doi.org/10.3847/1538-4357/ac4d29.

[7] S. Aiello, et al., gSeaGen: the KM3NeT GENIE-based code for neutrino telescopes, Comput. Phys. Commun. 256 (2020) 107477, https://doi.org/10.1016/j.cpc.2020.107477.

[8] P. Kalaczyński, The Measurement and Modelling of Cosmic Ray Muons at KM3NeT Detectors, Ph.D. thesis, University of Wuppertal, 2023.

[9] D. García-Fernández, A. Nelles, C. Glaser, Signatures of secondary leptons in radio-neutrino detectors in ice, Phys. Rev. D 102 (2020) 083011, https://doi.org/10.1103/PhysRevD.102.083011, arXiv:2003.13442.

[10] A. Fedynitch, W. Woodley, M.-C. Piro, On the accuracy of underground muon intensity calculations, Astrophys. J. 928 (2022) 27, https://doi.org/10.3847/1538-4357/ac5027, arXiv:2109.11559.

[11] M. Dunsch, et al., Recent improvements for the lepton propagator PROPOSAL, Comput. Phys. Commun. 242 (2019) 132–144, https://doi.org/10.1016/j.cpc.2019.03.021, arXiv:1809.07740.

[12] A. Sandrock, R.P. Kokoulin, A.A. Petrukhin, Theoretical uncertainties of muon transport calculations for very large volume neutrino telescopes, J. Phys. Conf. Ser. 1690 (2020) 012005, https://doi.org/10.1088/1742-6596/1690/1/012005.

[13] S.R. Kelner, R.P. Kokoulin, A.A. Petrukhin, Direct production muon pairs by high-energy muons, Phys. At. Nucl. 63 (2000) 1603–1611, https://doi.org/10.1134/1.1312894.

[14] A. Cooper-Sarkar, P. Mertsch, S. Sarkar, The high energy neutrino cross-section in the Standard Model and its uncertainty, J. High Energy Phys. 08 (2011) 042, https://doi.org/10.1007/JHEP08(2011)042, arXiv:1106.3723.

[15] I. Abt, et al., Investigation into the limits of perturbation theory at low Q^2 using HERA deep inelastic scattering data, Phys. Rev. D 96 (2017) 014001, https://doi.org/10.1103/PhysRevD.96.014001, arXiv:1704.03187.

[16] M.M. Block, L. Durand, P. Ha, Connection of the virtual $\gamma^* p$ cross section of ep deep inelastic scattering to real γp scattering, and the implications for νN and ep total cross sections, Phys. Rev. D 89 (2014) 094027, https://doi.org/10.1103/PhysRevD.89.094027, arXiv:1404.4530.

[17] A. Van Ginneken, Energy loss and angular characteristics of high-energy electromagnetic processes, Nucl. Instrum. Methods Phys. Res., Sect. A 251 (1986) 21–39, https://doi.org/10.1016/0168-9002(86)91146-0.

[18] S. Agostinelli, et al., GEANT4 – a simulation toolkit, Nucl. Instrum. Methods A 506 (2003) 250–303, https://doi.org/10.1016/S0168-9002(03)01368-8.

[19] Geant4 Collaboration, GEANT4 Physics Reference Manual, 11th edition, 2021, geant4.web.cern.ch.

[20] P. Gutjahr, Study of muon deflection angles in the TeV energy range with IceCube, Master's thesis, TU Dortmund University, 2021.

[21] P. Gutjahr, et al., Simulation of deflection uncertainties on directional reconstructions of muons using PROPOSAL, Eur. Phys. J. C 82 (2022) 1143, https://doi.org/10.1140/epjc/s10052-022-11102-5.

[22] T. Stanev, et al., Development of ultrahigh-energy electromagnetic cascades in water and lead including the Landau-Pomeranchuk-Migdal effect, Phys. Rev. D 25 (1982) 1291–1304, https://doi.org/10.1103/PhysRevD.25.1291.

[23] S. Polityko, et al., Muon cross-sections with both the LPM effect and the Ter-Mikayelyan effect at extremely high energies, J. Phys. G, Nucl. Part. Phys. 28 (2002) 427–449, https://doi.org/10.1088/0954-3899/28/3/306.

[24] A.A. Alves Junior, et al., Status of the novel CORSIKA 8 air shower simulation framework, Proc. Sci. 395 (2021) 284, https://doi.org/10.22323/1.395.0284, arXiv:2112.11761.

[25] R. Engel, et al., Towards a next generation of CORSIKA: a framework for the simulation of particle cascades in astroparticle physics, Comput. Softw. Big Sci. 3 (2019) 2, https://doi.org/10.1007/s41781-018-0013-0, arXiv:1808.08226.

[26] D. Heck, New Treatment of the Conversion $\gamma \to \mu^+ + \mu^-$ in CORSIKA, Tech. Rep. FZKA 7525, Forschungszentrum Karlsruhe, 2009.

[27] J.M. Hubbell, S.M. Seltzer, Tables of X-ray Mass Attenuation Coefficients and Mass Energy-Absorption Coefficients from 1 keV to 20 MeV for Elements Z = 1 to 92 and 48 Additional Substances of Dosimetric Interest, Tech. Rep. NISTIR 5632, National Institute of Standards and Technology, 1995.

[28] W.R. Nelson, H. Hirayama, D.W.O. Rogers, The EGS4 Code System, 1985.

[29] J.-M. Alameddine, et al., Electromagnetic shower simulation for CORSIKA 8, PoS ICRC2021 (2021) 428, https://doi.org/10.22323/1.395.0428.

[30] J.-M. Alameddine, A. Sandrock, F. Riehn, Validation of electromagnetic showers in CORSIKA 8, Proc. Sci. 444 (2023) 293, https://doi.org/10.22323/1.444.0393.

[31] N. Karastathis, et al., Simulating radio emission from air showers with CORSIKA 8, Proc. Sci. 444 (2023) 425, https://doi.org/10.22323/1.444.0425.

[32] F. Riehn, et al., Hadronic interaction model Sibyll 2.3d and extensive air showers, Phys. Rev. D 102 (2020) 063002, https://doi.org/10.1103/PhysRevD.102.063002.

[33] A. Mücke, et al., Monte Carlo simulations of photohadronic processes in astrophysics, Comput. Phys. Commun. 124 (2000) 290–314, https://doi.org/10.1016/S0010-4655(99)00446-4, arXiv:astro-ph/9903478.

[34] H.W. Koch, J.W. Motz, Bremsstrahlung cross-section formulas and related data, Rev. Mod. Phys. 31 (1959) 920–955, https://doi.org/10.1103/RevModPhys.31.920.

[35] Y.-S. Tsai, Pair production and bremsstrahlung of charged leptons, Rev. Mod. Phys. 46 (1974) 815–851, https://doi.org/10.1103/RevModPhys.46.815.

[36] J.W. Motz, H.A. Olsen, H.W. Koch, Pair production by photons, Rev. Mod. Phys. 41 (1969) 581–639, https://doi.org/10.1103/RevModPhys.41.581.

[37] M. Sackel, et al., CubicInterpolation, https://github.com/tudo-astroparticlephysics/cubic_interpolation, Nov. 2021.

[38] G. Melman, spdlog, https://github.com/gabime/spdlog, Nov. 2022.

[39] N. Lohmann, JSON for Modern C++, https://github.com/nlohmann, Aug. 2022.

[40] W. Jakob, J. Rhinelander, D. Moldovan, pybind11 – Seamless operability between C++11 and Python, https://github.com/pybind/pybind11, 2017.

[41] The Conan team, Conan, https://docs.conan.io/en/1.44/conan.pdf, Mar. 2023.

[42] Python Package Index - PyPI, https://pypi.org/.

[43] J.-M. Alameddine, et al., PROPOSAL: a library to propagate leptons and high energy photons, J. Phys. Conf. Ser. 1690 (2020) 012021, https://doi.org/10.1088/1742-6596/1690/1/012021.

[44] G. Guennebaud, B. Jacob, et al., Eigen v3, http://eigen.tuxfamily.org, 2010.

[45] B. Schling, The Boost C++ Libraries, XML Press, 2011.

[46] M. Chrzaszcz, et al., TAUOLA of τ lepton decays—framework for hadronic currents, matrix elements and anomalous decays, Comput. Phys. Commun. 232 (2018) 220–236, https://doi.org/10.1016/j.cpc.2018.05.017, arXiv:1609.04617.

[47] F.D. Aaron, et al., Combined measurement and QCD analysis of the inclusive $e^{\pm}$p scattering cross sections at HERA, J. High Energy Phys. 01 (2010) 109, https://doi.org/10.1007/JHEP01(2010)109, arXiv:0911.0884.

[48] A. Cooper-Sarkar, Proton structure from HERA to LHC, pp. 277–284, arXiv:1012.1438, https://www.desy.de/h1zeus/combined_results/herapdftable/, 2010.

[49] H. Abramowicz, et al., A parametrization of $\sigma_T(\gamma^* p)$ above the resonance region for $q^2 \geq 0$, Phys. Lett. B 269 (1991) 465–476, https://doi.org/10.1016/0370-2693(91)90202-2.

[50] H. Abramowicz, et al., Combination of measurements of inclusive deep inelastic $e^{\pm}p$ scattering cross sections and QCD analysis of HERA data, Eur. Phys. J. C 75 (2015) 580, https://doi.org/10.1140/epjc/s10052-015-3710-4.

[51] M.R. Adams, et al., Proton and deuteron structure functions in muon scattering at 470 GeV, Phys. Rev. D 54 (1996) 3006–3056, https://doi.org/10.1103/PhysRevD.54.3006.

[52] M. Arneodo, et al., Measurement of the proton and deuteron structure functions, f_2^p and f_2^d, and of the ratio σ_L/σ_T, Nucl. Phys. B 483 (1997) 3–43, https://doi.org/10.1016/S0550-3213(96)00538-X.

[53] A.C. Benvenuti, et al., A high statistics measurement of the proton structure functions $f_2(x, q^2)$ and r from deep inelastic muon scattering at high q^2, Phys. Lett. B 223 (1989) 485–489, https://doi.org/10.1016/0370-2693(89)91637-7.

[54] M.M. Block, F. Halzen, Evidence for the saturation of the Froissart bound, Phys. Rev. D 70 (2004) 091901(R), https://doi.org/10.1103/PhysRevD.70.091901.

[55] S.R. Kelner, Pair production in collisions between a fast particle and a nucleus, Sov. J. Nucl. Phys. 5 (5) (1967) 778–783.

[56] R.P. Kokoulin, A.A. Petrukhin, Analysis of the cross-section of direct pair production by fast muons, in: Proceedings of the 11th International Conference on Cosmic Rays (ICCR 1969), vol. 4, 1969, pp. 277–284.

[57] V.V. Borog, V.G. Kirillov-Ugryumov, A.A. Petrukhin, Inelastic interaction of muons with Fe nuclei at small Q^2 in the energy region above 200 GeV, Sov. J. Nucl. Phys. 25 (1) (1977), https://www.osti.gov/biblio/7308048.

[58] V. Borog, A. Petrukhin, The cross-section of the nuclear interaction of high energy muons, in: International Cosmic Ray Conference, in: International Cosmic Ray Conference, vol. 6, 1975, pp. 1949–1954.
[59] J.D. Bjorken, Inequality for backward electron- and muon-nucleon scattering at high momentum transfer, Phys. Rev. 163 (1967) 1767–1769, https://doi.org/10.1103/PhysRev.163.1767.
[60] M.J. Berger, S.M. Seltzer, Tables of energy losses and ranges of electrons and positrons, Tech. Rep. NASA SP-3012, National Aeronautics and Space Administration, 1964.
[61] R.M. Sternheimer, R.F. Peierls, General expression for the density effect for the ionization loss of charged particles, Phys. Rev. B 3 (1971) 3681–3692, https://doi.org/10.1103/PhysRevB.3.3681.
[62] H. Hirayama, et al., The EGS5 code system, Tech. Rep., Stanford Linear Accelerator Center (SLAC), 2005.
[63] J. Butcher, H. Messel, Electron number distribution in electron-photon showers in air and aluminium absorbers, Nucl. Phys. 20 (1960) 15–128, https://doi.org/10.1016/0029-5582(60)90162-0.
[64] H. Davies, H.A. Bethe, L.C. Maximon, Theory of bremsstrahlung and pair production. II. Integral cross section for pair production, Phys. Rev. 93 (1954) 788–795, https://doi.org/10.1103/PhysRev.93.788.
[65] S. Duane, A. Bielajew, D.W.O. Rogers, Use of ICRU-37/NBS collision stopping powers in the EGS4 system, Tech. Rep. PIRS-0173, National Research Council Canada, 1989, https://people.physics.carleton.ca/~drogers/pubs/papers/pirs173.pdf.
[66] M.J. Berger, et al., Stopping powers for electrons and positions, (ICRU Report No. 37), J. Int. Comm. Radiat. Units Meas. 2 (1984), https://doi.org/10.1093/jicru/os19.2.Report37.
[67] W. Heitler, The Quantum Theory of Radiation, 3rd edition, Oxford University Press, 1954.
[68] O. Klein, Y. Nishina, Über die Streuung von Strahlung durch freie Elektronen nach der neuen relativistischen Quantendynamik von Dirac, Z. Phys. 52 (1929) 853–868, https://doi.org/10.1007/BF01366453.
[69] L. Storm, H.I. Israel, Photon cross sections from 1 keV to 100 MeV for elements $Z = 1$ to $Z = 100$, At. Data Nucl. Data Tables 7 (1970) 565–681, https://doi.org/10.1016/S0092-640X(70)80017-1.
[70] S. Klein, Suppression of bremsstrahlung and pair production due to environmental factors, Rev. Mod. Phys. 71 (1999) 1501–1538, https://doi.org/10.1103/RevModPhys.71.1501.
[71] A.B. Migdal, Bremsstrahlung and pair production in condensed media at high energies, Phys. Rev. 103 (1956) 1811–1820, https://doi.org/10.1103/PhysRev.103.1811.
[72] S.R. Kelner, R.P. Kokoulin, A.A. Petrukhin, About cross section for high-energy muon bremsstrahlung, Tech. Rep. MEPHI-95-24, 1995, https://cds.cern.ch/record/288828.
[73] S.R. Kelner, R.P. Kokoulin, A.A. Petrukhin, Radiation logarithm in the Hartree-Fock model, Phys. At. Nucl. 62 (1999) 1894–1898.
[74] F. Sauter, Über den atomaren Photoeffekt bei großer Härte der anregenden Strahlung, Ann. Phys. 401 (1931) 217–248, https://doi.org/10.1002/andp.19314010205.
[75] F. Sauter, Über den atomaren Photoeffekt in der K-Schale nach der relativistischen Wellenmechanik Diracs, Ann. Phys. 403 (1931) 454–488, https://doi.org/10.1002/andp.19314030406.
[76] J.H. Hubbell, Photon Cross Sections, Attenuation Coefficients, and Energy Absorption Coefficients from 10 keV to 100 GeV, Tech. Rep. NSRDS-NBS 29, National Bureau of Standards, 1969.
[77] A. Bielajew, R. Mohan, C.-S. Chui, Improved bremsstrahlung photon angular sampling in the EGS4 code system, Tech. Rep. PIRS-0203, National Research Council Canada, 1989.
[78] H. Abramowicz, A. Levy, The ALLM parametrization of $\sigma_{\text{tot}}(\gamma^* p)$, an update, arXiv:hep-ph/9712415, 1997.
[79] A.V. Butkevich, S.P. Mikheyev, Cross section of the muon-nuclear inelastic interaction, J. Exp. Theor. Phys. 95 (2002) 11–25, https://doi.org/10.1134/1.1499897, arXiv:hep-ph/0109060.
[80] W. Rhode, Untersuchung der Energiespektren hochenergetischer Muonen im Fréjus-detektor, Ph.D. thesis, University of Wuppertal, 1993.
[81] R.P. Kokoulin, A.A. Petrukhin, Influence of the nuclear formfactor on the cross-section of electron pair production by high energy muons, in: Proceedings of the 12th International Conference on Cosmic Rays (ICCR 1971), vol. 4, 1971, pp. 2436–2444.
[82] S.R. Kelner, Pair production in collisions between muons and atomic electrons, Phys. At. Nucl. 61 (1998) 448–456.
[83] H. Bethe, Zur Theorie des Durchgangs schneller Korpuskularstrahlen durch Materie, Ann. Phys. 397 (1930) 325–400, https://doi.org/10.1002/andp.19303970303.
[84] B. Rossi, W.B. Fretter, High-energy particles, Am. J. Phys. 21 (1953) 236, https://doi.org/10.1119/1.1933408.